Stokes Polarimetry in He I 10830: Magnetic Field Topology of an Emerging Flux Region

Andreas Lagg

Max-Planck-Institute for Solar System Research, Germany

Outline:

- Chromospheric magnetic field measurements
  - relevance & previous methods
- The He 10830 diagnostics
  - Zeeman, scatter polarization, Hanle
  - line formation
  - implementation
- Application: emerging flux region
  - parameter maps, loop tracing, 3D-structure of chromosphere
  - fast downflow region
- Summary

The missing link

tough: coronal magnetic field structure

- TRACE: Loops
- radio methods
- very sensitive Zeeman diagnostics (Fe XIII 10747, Lin et al., 2004)
- coronal seismology (dispersion relation of magnetoacoustic kink mode, Nakariakov & Ofman, 2001)

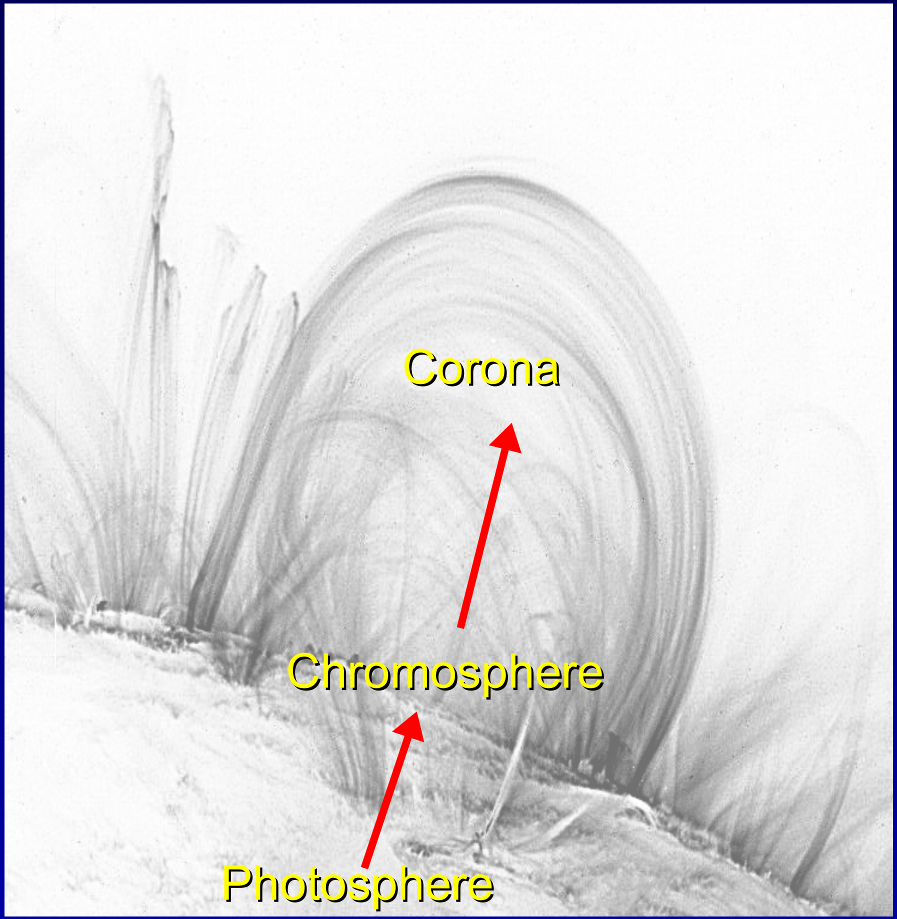

'easy': photospheric field
(Zeeman diagnostics)

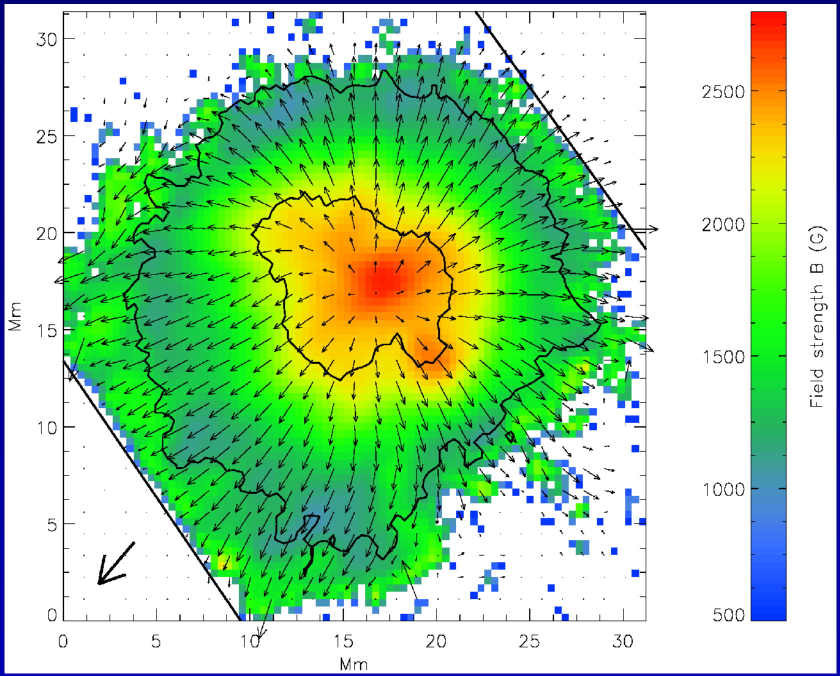

(Mathew, 2003)

Relevance of chromospheric magnetic field measurements

- transition: plasma dominated region (β>1) to magnetic field dominated region
- Magnetic connection between photosphere and corona?
- Is there the concept of "magnetic canopy" correct?
  - weak, volume-filling field (Faurobert, 2001) or compact regions with kG field (e.g. Sanchez-Almeida, 2003)?
  - is the weak intranetwork field entirely cut off from the outer atmosphere?
- Chromospheric / Coronal Heating (DC/ wave heating)

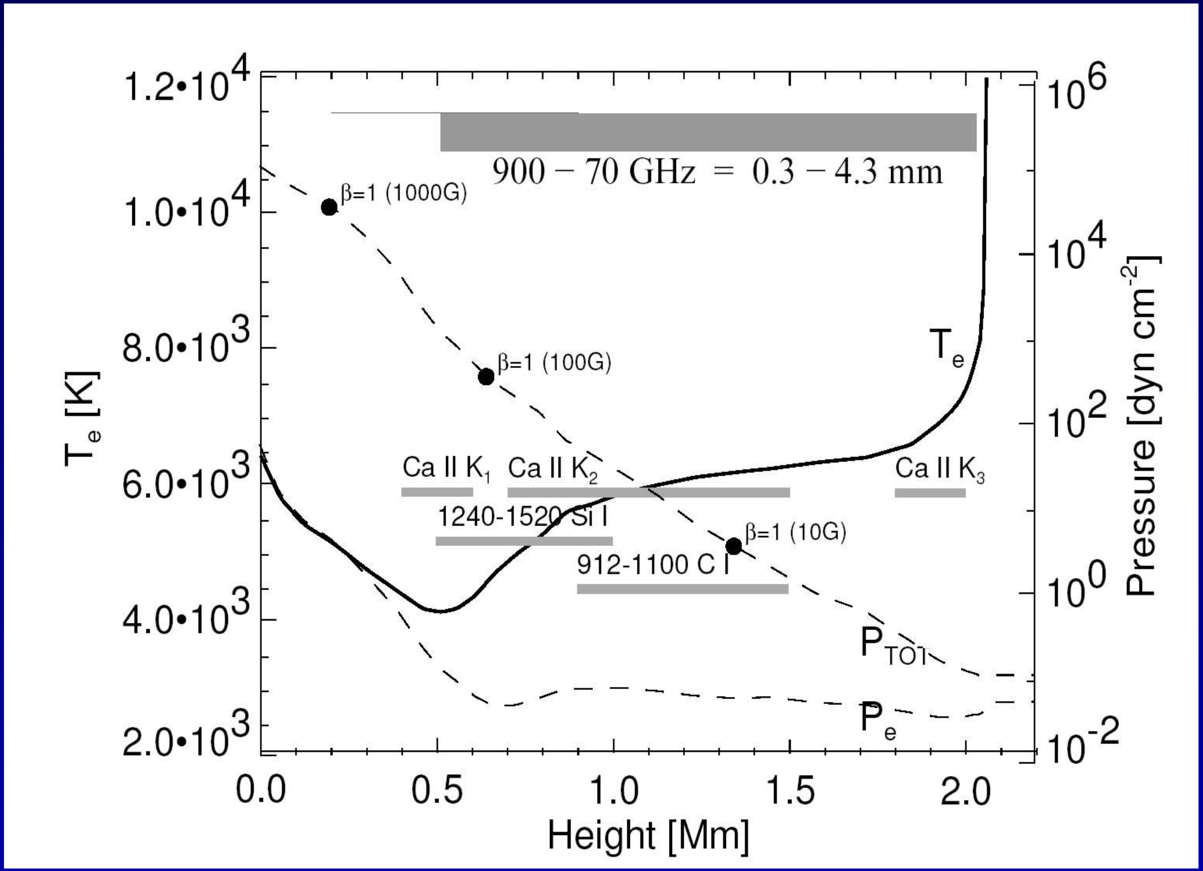

H. Peter (2002)

Relevance: Coronal Heating

- heating mechanism located below 10 Mm above photosphere (Aschwanden et al., 2001)
- footpoint heating models (incomplete):
  - Sakai et al. (2001): magnetic reconnection resulting from surface Alfvén waves and colliding plasma flows in chromospheric current sheets
  - colliding flux tubes in the chromosphere (Ryutova, 2001)
  - interaction of newly emerging loops with pre-existing loops (Mok, 2001)

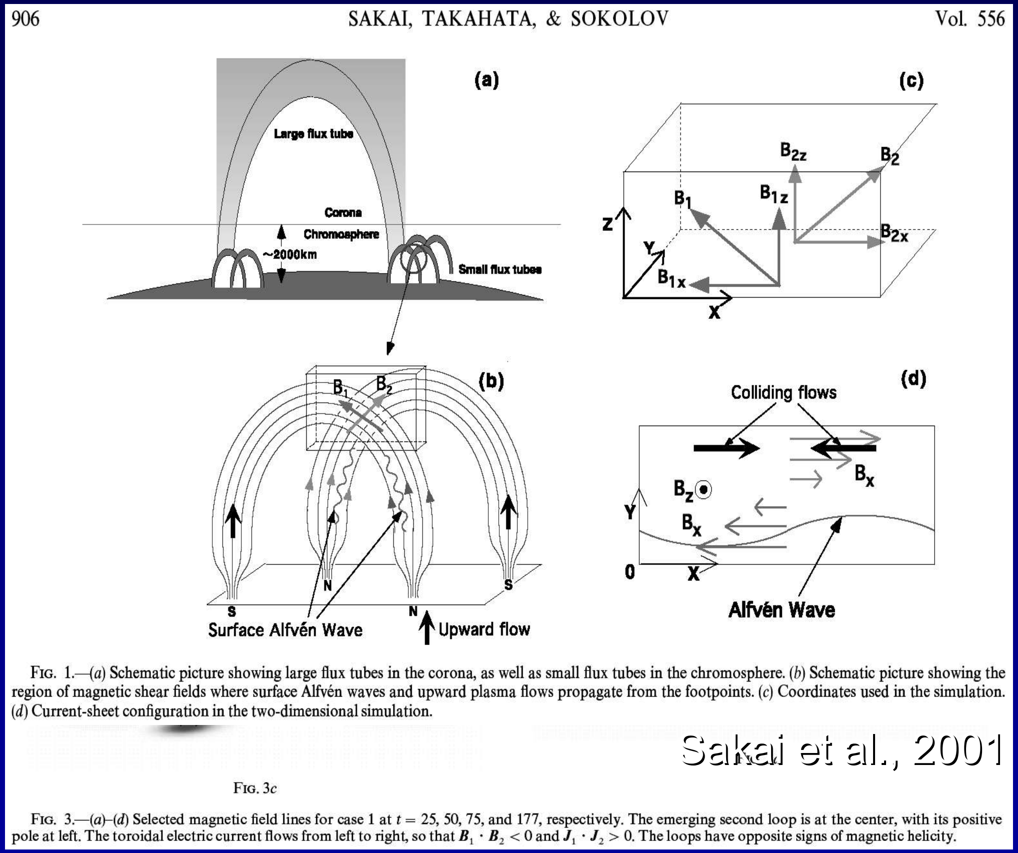

FIG. 1.—(a) Schematic picture showing large flux tubes in the corona, as well as small flux tubes in the chromosphere. (b) Schematic picture showing the region of magnetic shear fields where surface Alfvén waves and upward plasma flows propagate from the footpoints. (c) Coordinates used in the simulation. (d) Current-sheet configuration in the two-dimensional simulation.

FIG. 3.—(a)–(d) Selected magnetic field lines for case 1 at $t = 25, 50, 75$, and 177, respectively. The emerging second loop is at the center, with its positive pole at left. The toroidal electric current flows from left to right, so that $B_1 \cdot B_2 < 0$ and $J_1 \cdot J_2 > 0$. The loops have opposite signs of magnetic helicity.

Mok, 2001

"The ultimate test of any coronal heating model requires a detailed one-to-one correspondence of changes in magnetic features with the locations of coronal heating input." (Trimble & Aschwanden, 2002)

Previous methods (1)

Extrapolations

use reliable photospheric data

e.g. Seehafer & Staude (1979):

Force free magnetic field extrapolations:

$$\nabla \times \vec{B} = \alpha B$$

comparison with Hα features:

force-free (α = const) superior to current-free (α = 0)

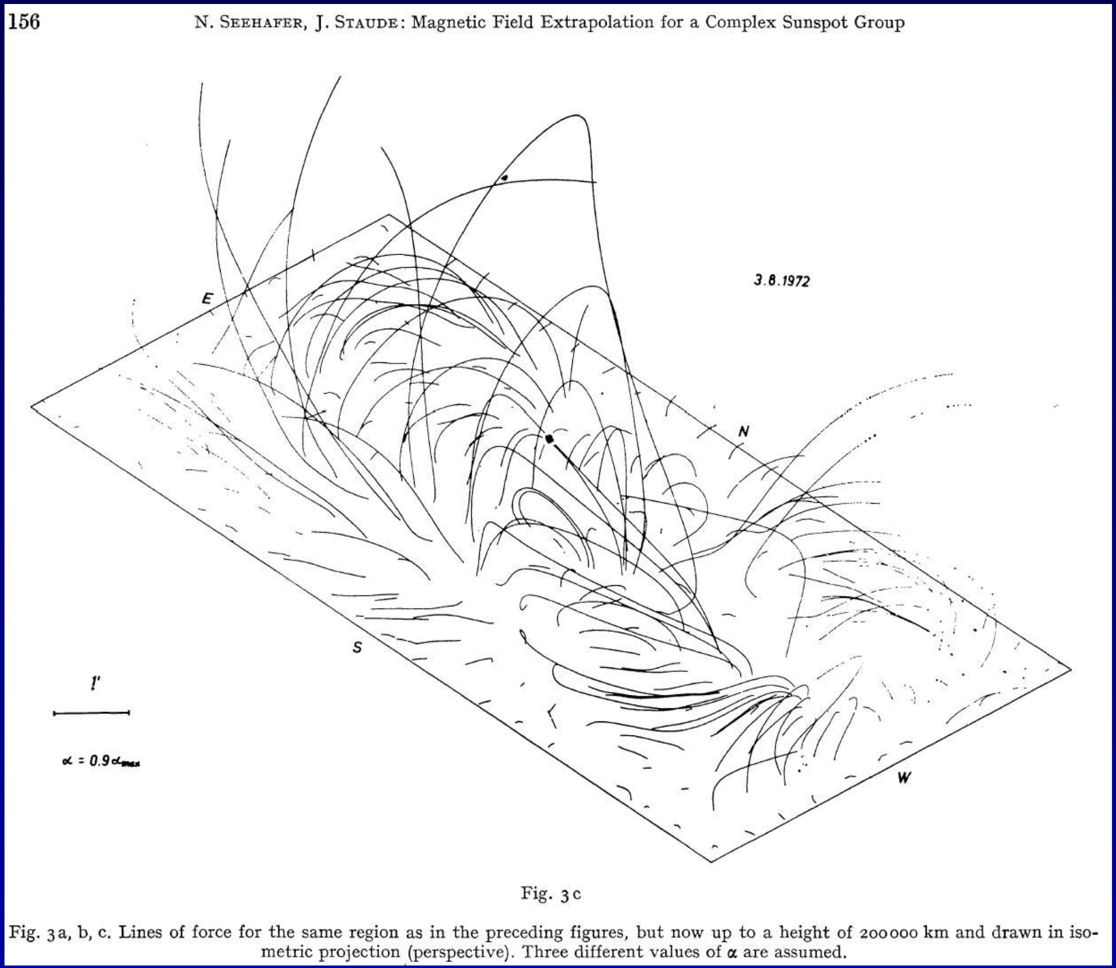

(Yan & Sakurai (1997): comparison with YOHKOH, Régnier et. al (2002): non constant α)

Previous methods (2)

Radio Emissions

e.g. S. M. White (2002)

- depend directly on magnetic field at origin
- uses gyroresonant emissions, bremsstrahlung
- no information on magnetic field direction
- only for moderate strong fields (> few hundred Gauss)
- low temporal and spatial details

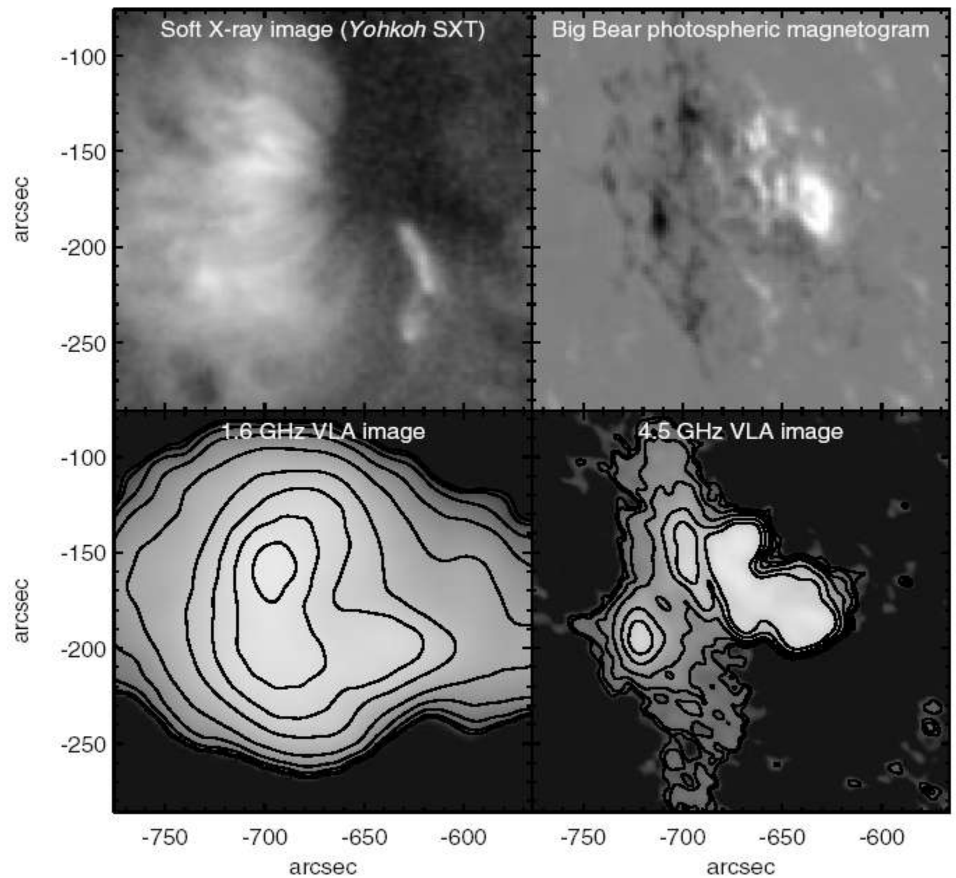

Fig. 2. Contrast in the appearance of a solar active region (1992 April 11). A soft X-ray image (Yohkoh/SXT) is shown in the top left panel, a longitudinal magnetogram in the top right panel, and two VLA radio images are shown in the lower panels: a 1.6 GHz image at left, and a 4.5 GHz image at right. Note the striking difference in the radio images: at the lower frequency the radio image is dominated by optically-thick bremsstrahlung from the loops visible in the soft X-ray image. At the higher frequency this emission is optically thin, and the image is dominated instead by gyroresonance emission from the strong magnetic fields in the corona above the active region.

The HeI 10830 diagnostics (1)

Zeeman Effect

- reliable magnetic field information for B >100 G
- simultaneous observation of photosphere (Si) and chromosphere (He)
- three (blended) HeI lines ("blue" line + 2 "red" lines)

Atomic Parameters: [Rüedi, 1996]

Line	WL [Å]	Transition	g_{eff}	ROS
Si I	10827.14	4s $^3P_2$ - 4p $^3P_2$	1.50	
He I	10828.99	2s $^3S_1$ - 2p $^3P_0$	2.00	0.111
He I	10830.38	2s $^3S_1$ - 2p $^3P_1$	1.75	0.333
He I	10830.38	2s $^3S_1$ - 2p $^3P_2$	0.875	0.556

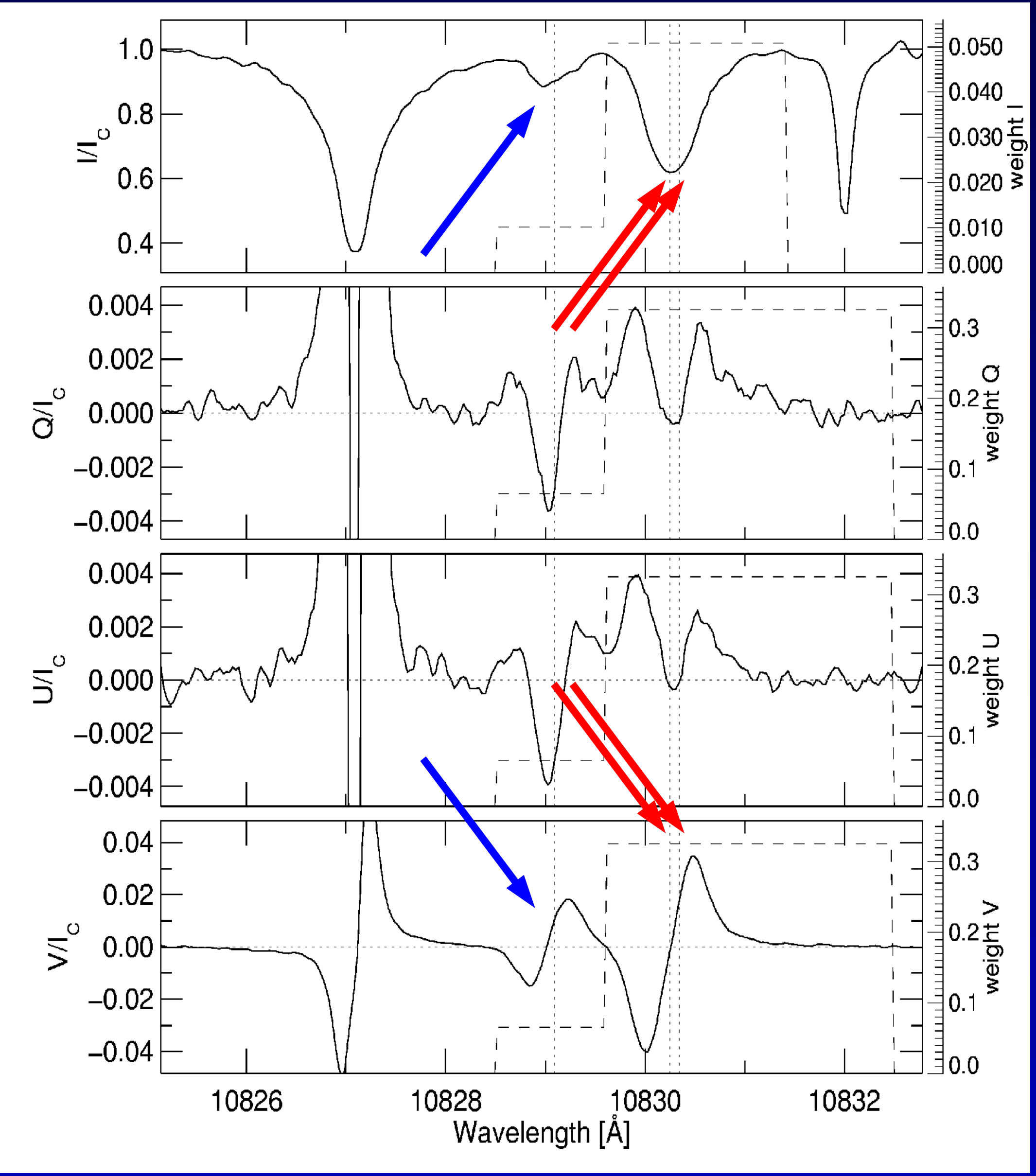

The HeI 10830 diagnostics (2)

Hanle Effect

(Trujillo-Bueno, 2002,

Landi Degl'Innocenti, 1982)

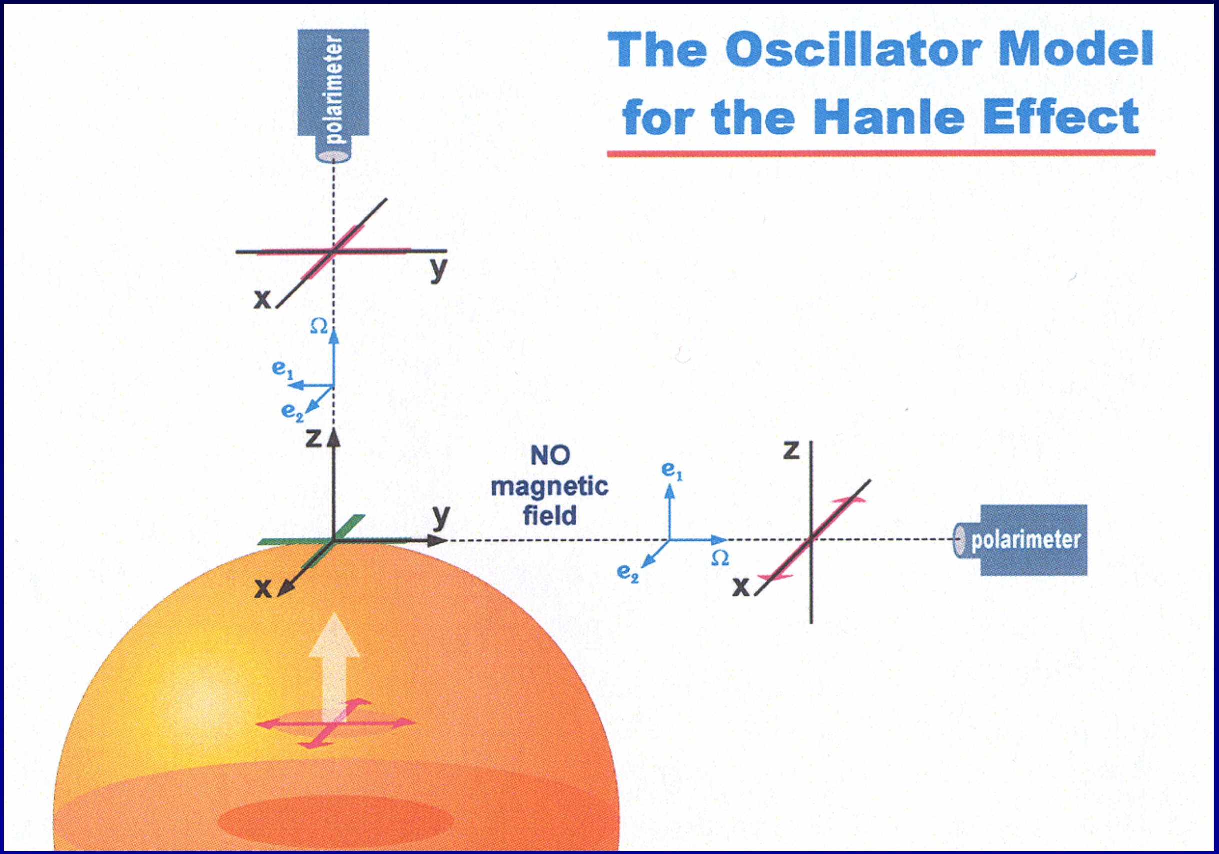

non magnetic case:
anisotropic illumination of atoms (3 independent, damped oscillators in x,y,z) with unpolarized light

- no polarization in forward scattering
- complete linear polarization in 90° scattering

→ ***scattering polarization***

Hanle effect:
modification of (atomic) polarization caused by the action of a magnetic field

The HeI 10830 diagnostics (2)

Hanle Effect

(Trujillo-Bueno, 2002,

Landi Degl'Innocenti, 1982)

magnetic case:
now the 3 oscillators are not independent:

- 1 osc. along B (ω_0)
- 2 osc. around B (ω_0-ω_L ; ω_0+ω_L)
- damped oscillation precesses around B
  → rosette like pattern
  → damping time $t_{life} = 1/\gamma$

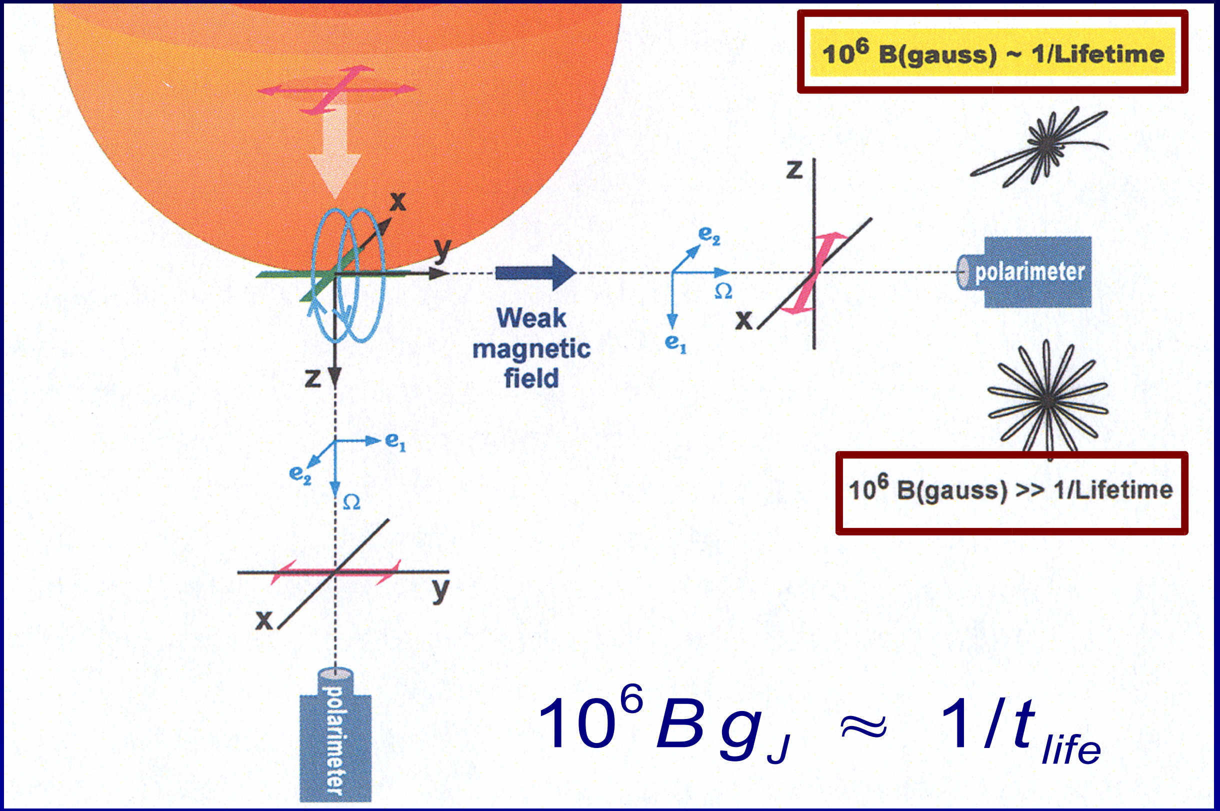

- $\omega_B >> 1/t_{life}$
  - forward scattering: max. polarization along ±y
  - 90° scattering: no polarization

- $\omega_B \approx 1/t_{life}$
  - forward scattering: weaker, but still ±y
  - 90° scattering: lin.pol. in Q, U, smaller than in non-magnetic case

The HeI 10830 diagnostics (2)

Hanle Effect, the He 10830 case

'normal' case: upper level atomic polarization

Transition:

$J = 0 \rightarrow 1 \rightarrow 0$

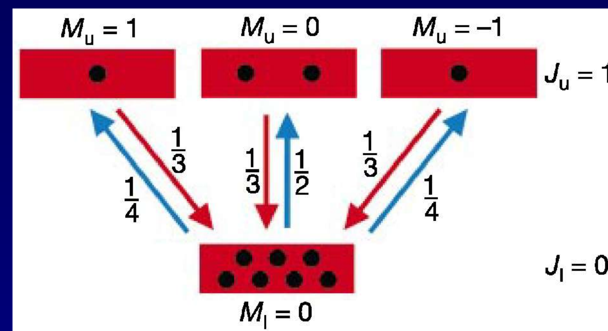

Blue Line (J_L=1, J_U=0): degenerate lower level

- upper level cannot carry atomic polarization
  → emitted beam to (1) unpolarized
  → transmitted beam (2) has excess of linear polarization ⊥ to B (=dichroism)

Red Lines (J_L=1, J_U=2 and J_L=1, J_U=1): degenerate upper & lower level

- both levels carry atomic polarization
  → emitted beam to (1) polarized
  → transmitted beam (2) has excess of linear polarization ⊥ to B

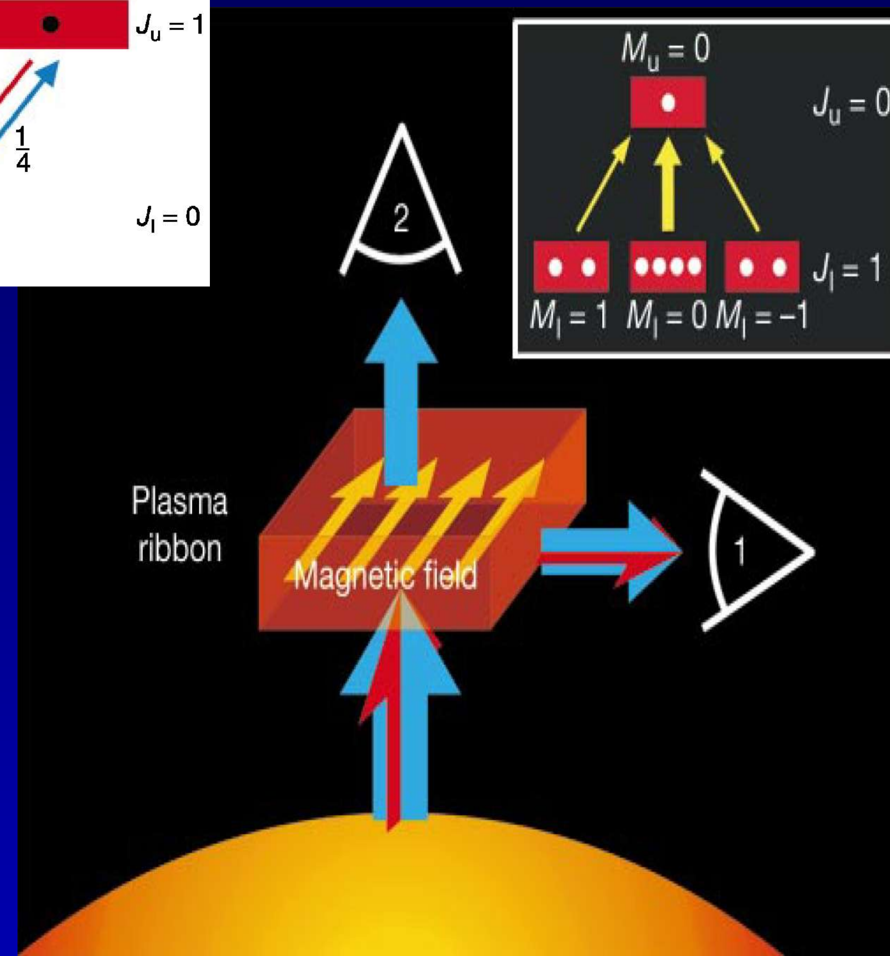

Trujillo-Bueno, 2002

The prominence case:
(90° scattering)
linear polarization only in red line

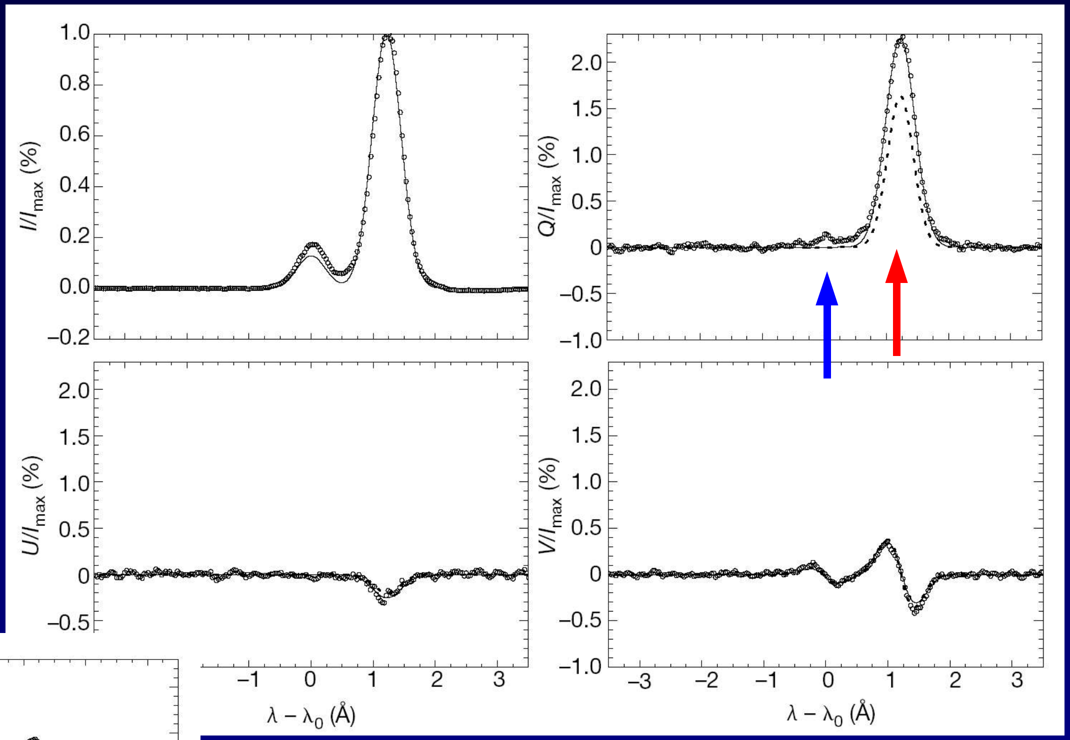

Trujillo-Bueno, 2001

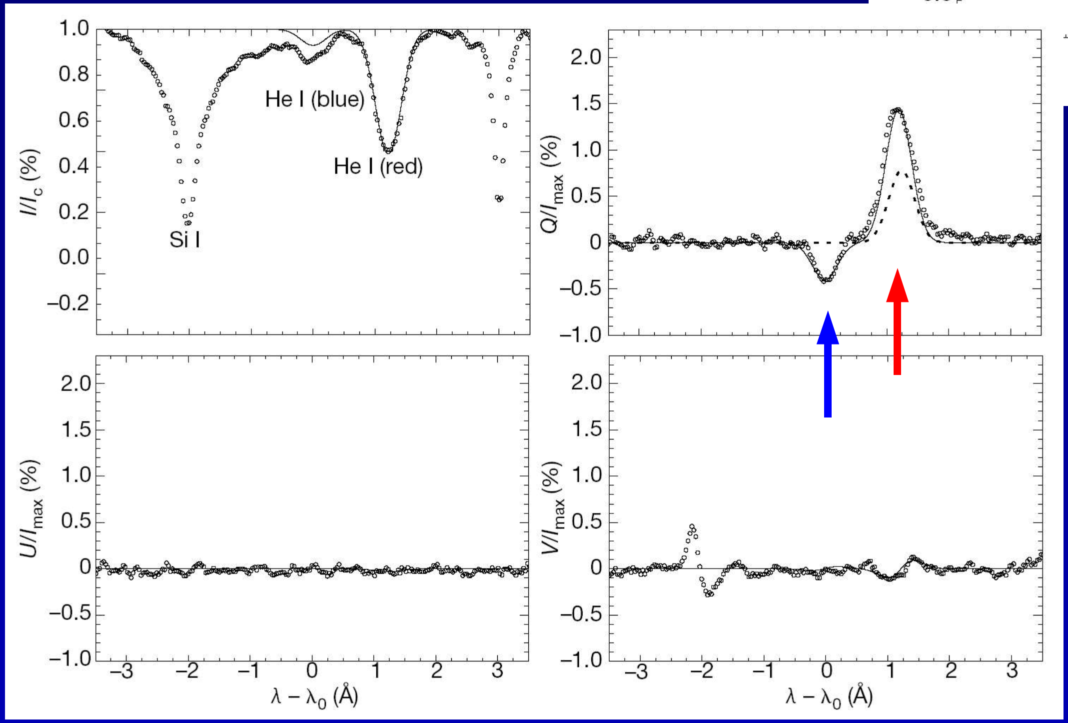

The filament case:
(forward scattering)
linear polarization in
red & blue line

Si / He Line Formation

Si 1082.7 nm (photosphere)

- formed in photosphere (LTE)
- moderate magnetic field and temperature sensitivity
- Maxwellian local velocity distribution
- SPINOR (Frutiger 2000)

He 1083 nm Triplet (upper chromosphere)

- good magnetic field sensitivity
- non-LTE formation (h>1500 km)
- complex formation (Avrett 1994)
- optically thin (Rüedi 1995)
  - no complicated RT-calc
  - no details of line formation

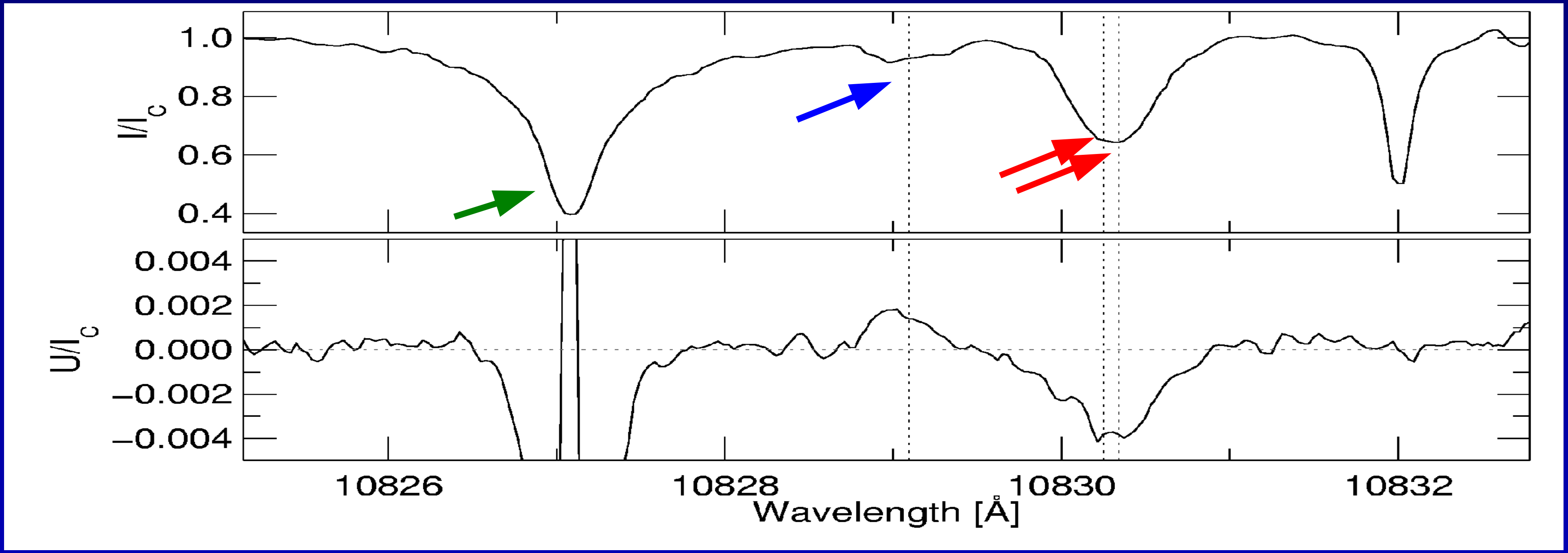

Analysis Technique for HeI 10830

- forward calculation (synthesis) involving
  - radiative transfer
  - Zeeman effect
  - Hanle effect
  - multiple atmospheric components
- Inversion technique
  - weighting scheme
  - robustness

Synthesis of HeI Spectra (1)

non-LTE line formation → SPINOR not applicable

first step: simple Gaussian fit to individual Zeeman components

improvement: include basics of radiative transfer

$$\frac{d\mathbf{I}}{dz} = -\mathbf{K}\,\mathbf{I}$$

K= propagation matrix (contains absorption and dispersion profiles, eg. η_V)

$$\eta_V = \left(\frac{\eta_r - \eta_b}{2}\right)\cos\gamma, \quad \eta_{b,r} = \eta_0 H(a, \lambda - \Delta\lambda_{vLOS} \pm \Delta\lambda_B)$$

Free parameters: amplitude η_0, damping constant a, LOS-velocity (v_{LOS}), Doppler broadening ($\Delta\lambda_D$), magnetic field strength & direction (B, φ, γ)

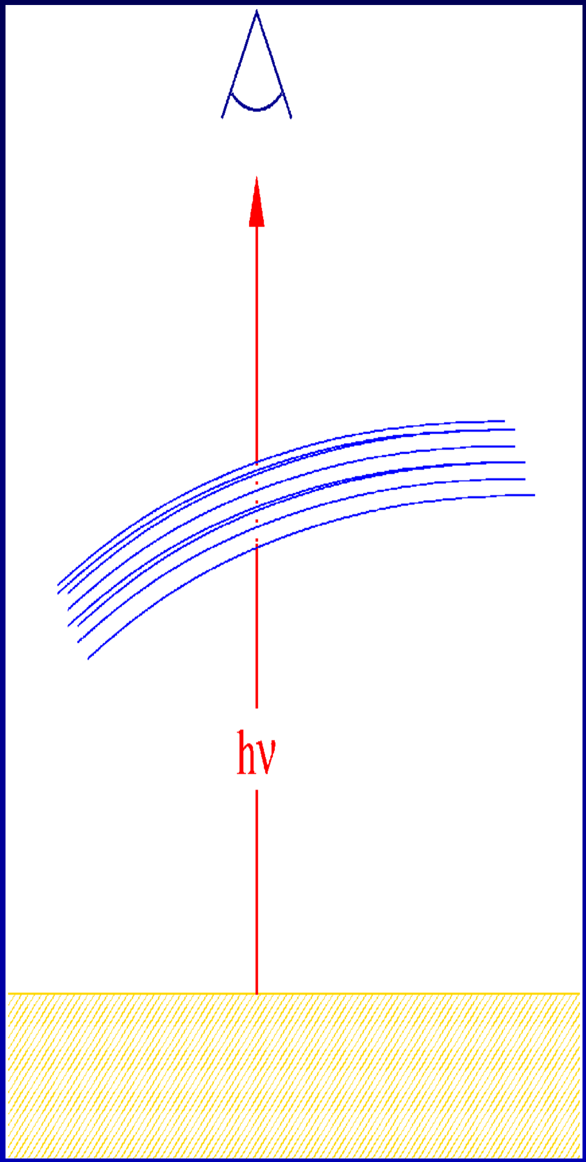

Synthesis of HeI Spectra (2)

radiative transfer: Milne-Eddington approximation

- height independent prop. matrix **K**
- all quantities of atmosphere are constant with optical depth, except for source function:

$$S(\tau) = S_0 + S_1 \tau$$

Additional free parameters: S_1

→ 8 free parameters defining one atmospheric component

He-Triplet: all three lines formed under identical conditions

→ same atmospheric parameters

→ linear coupling using rel. oscillator strength

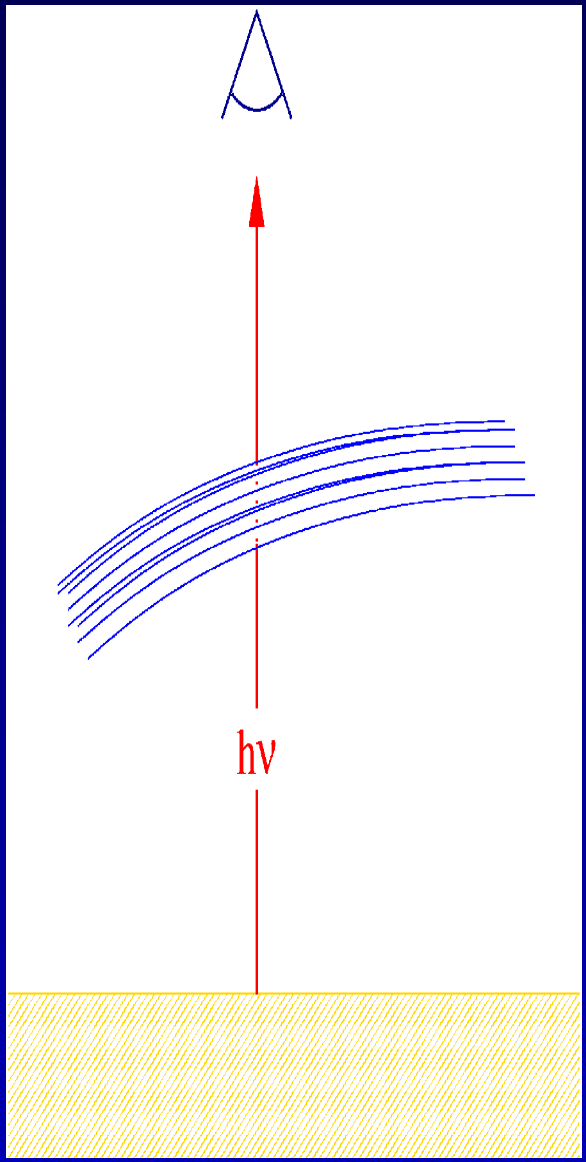

Implementation of Hanle (1)

regions with strong linear polarization

→ no Zeeman fit possible

'filament case' for scatter-polarization:

- B-field ∥ solar surface
- LOS ⊥ solar surface

$$\Rightarrow \quad \tan(2\chi) = U/Q$$

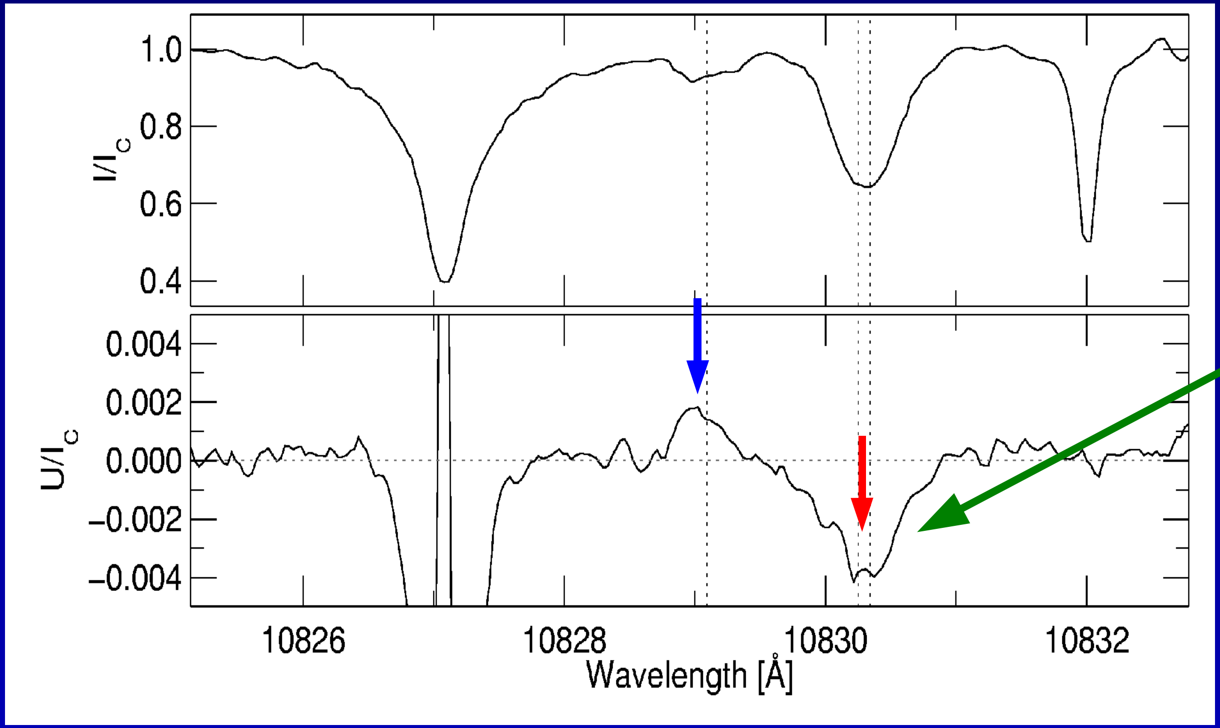

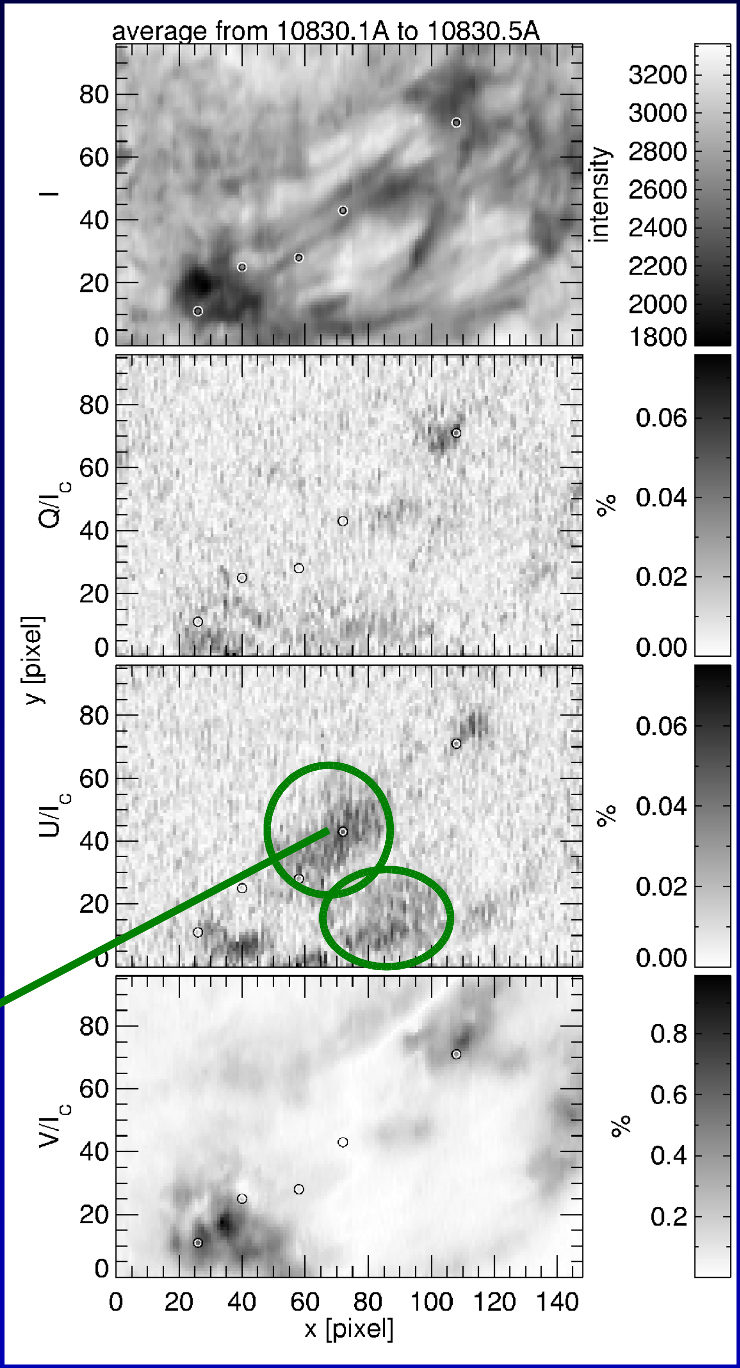

Implementation of

- fit Voigt to Sokes I
- assume same shape for scatt
  pol. signal (v_{LOS}, line width)

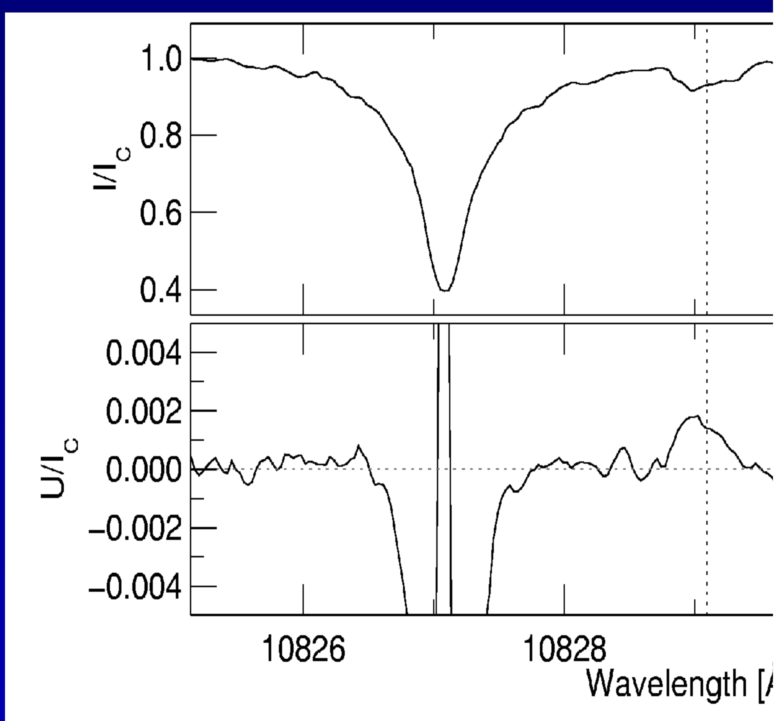

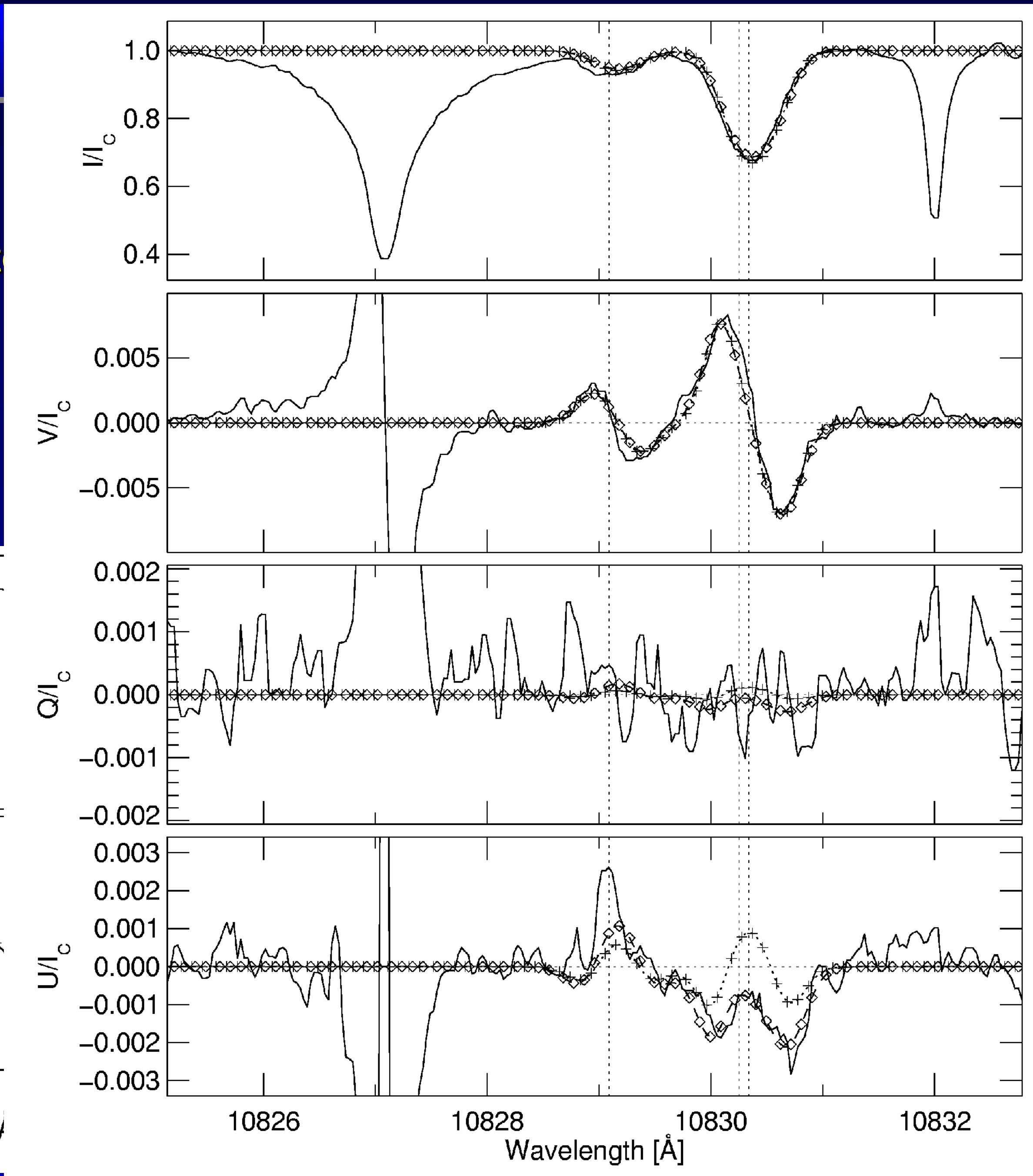

Multi-Component Analysis

some pixels: single atmosphere not able to reproduce observed profile

→ introduce 2nd component

parameter coupling helps to reduce number of free parameters
(e.g. couple magnetic field direction)

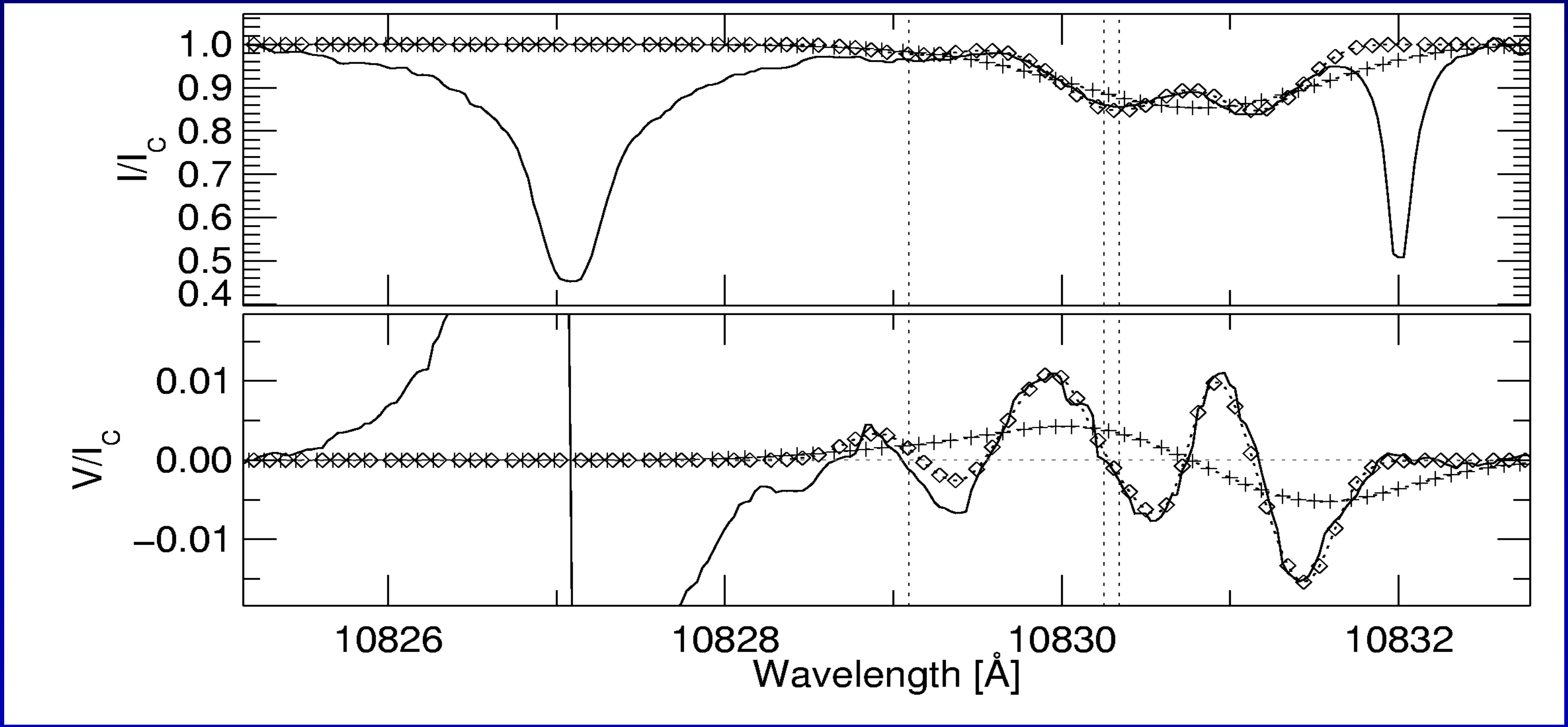

Weighting Scheme

telluric blend: Stokes I up to 10831.5 Å

photospheric Ca-line blends blue HeI line → reduced weight

Stokes Q, U, V: similar to I, no blend

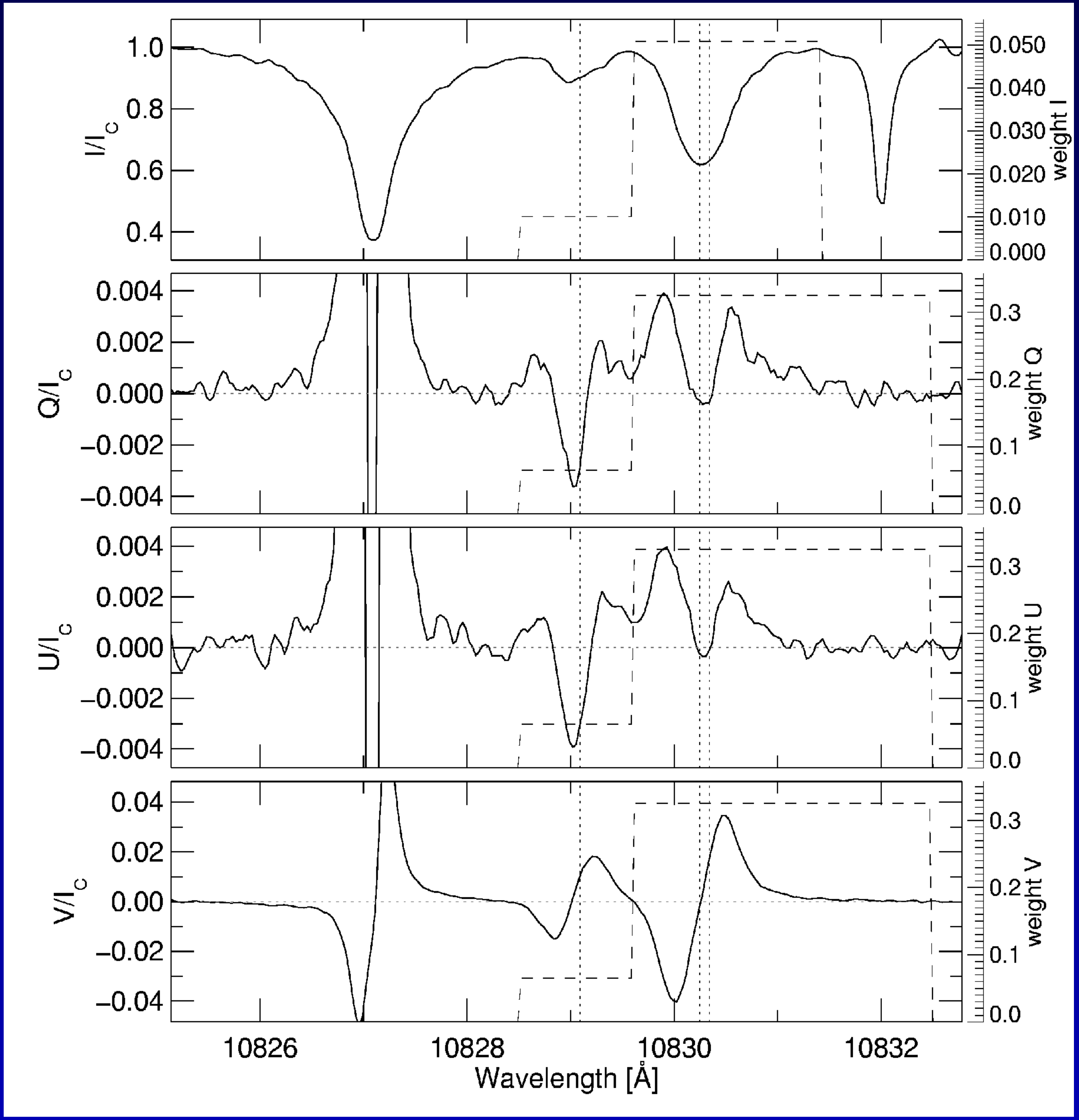

Inversion Technique

- robustness:
  - steepest gradient (UOBYQA)
  - genetic algorithm (PIKAIA)
- multi-iteration technique:
  - first fit reliable parameters (eg. v_{LOS})
  - reduced number of free parameters for 2^{nd} run

Pikaia

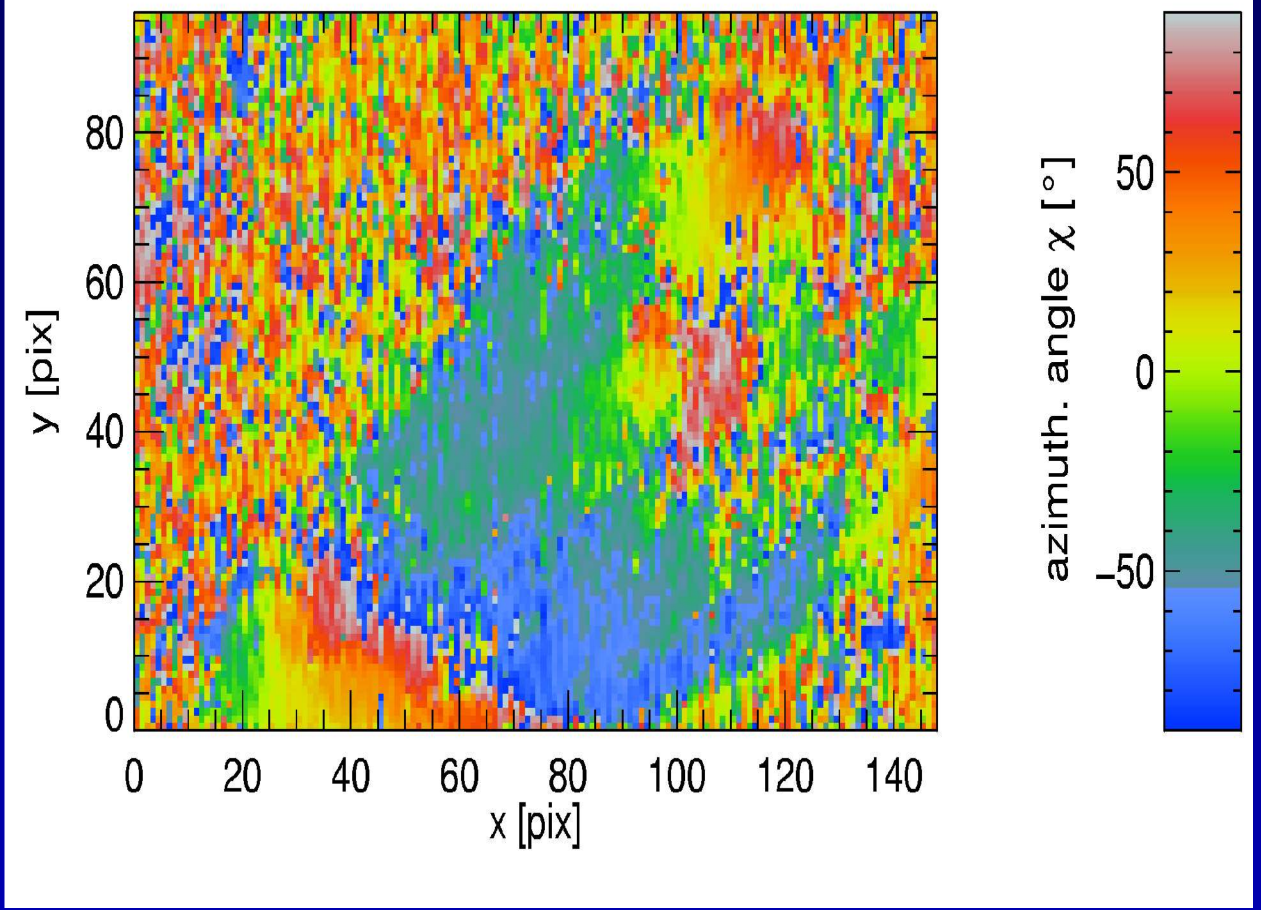

Convergence and Noise Analysis

weak field

inclination

azimuth

strong field

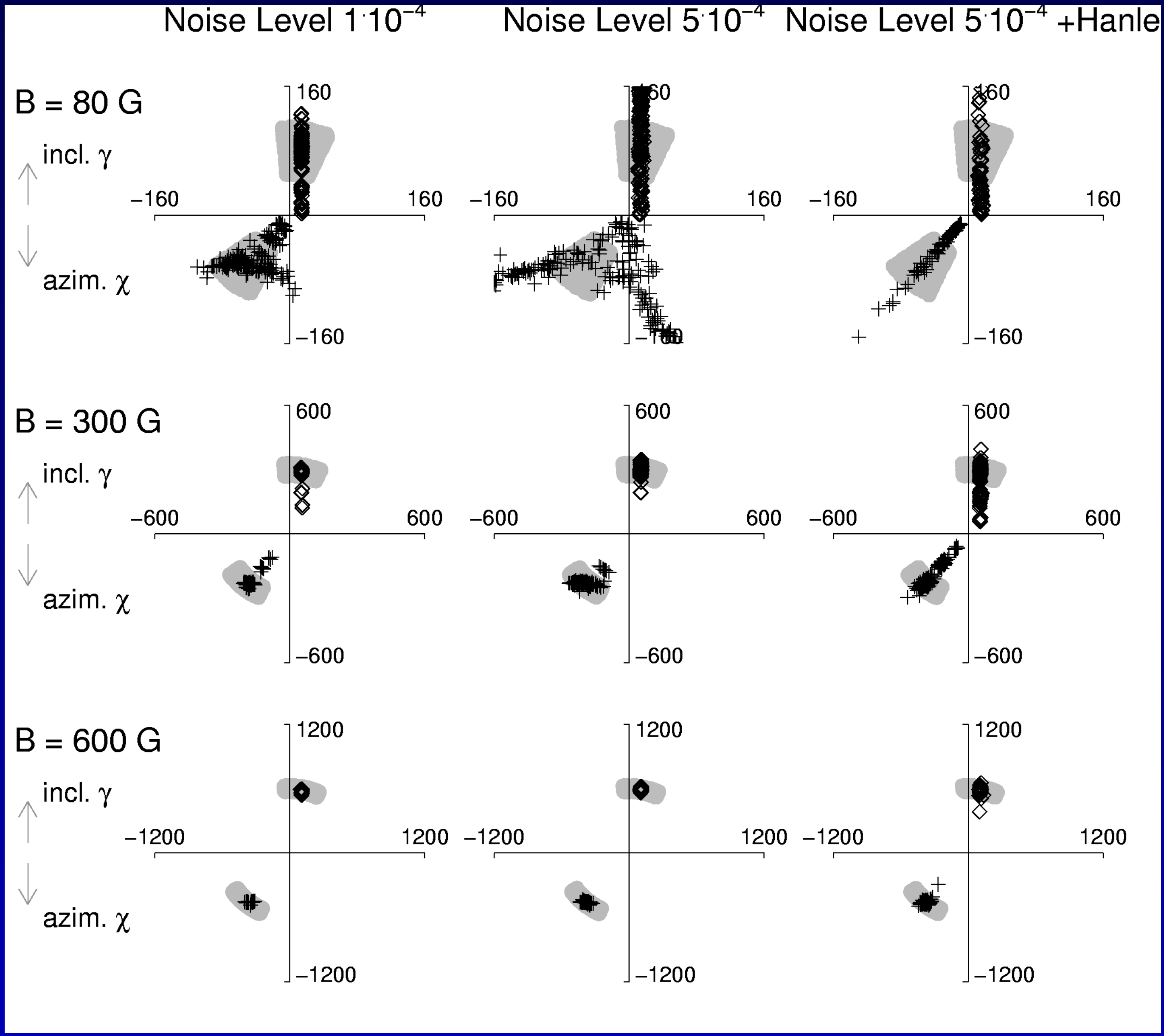

Data Set

VTT / TIP

- Spect
  29 mÅ /
- Spatial res
  0.4" / pix
- Integration ti
  5s / slit
- scan perp. to slit

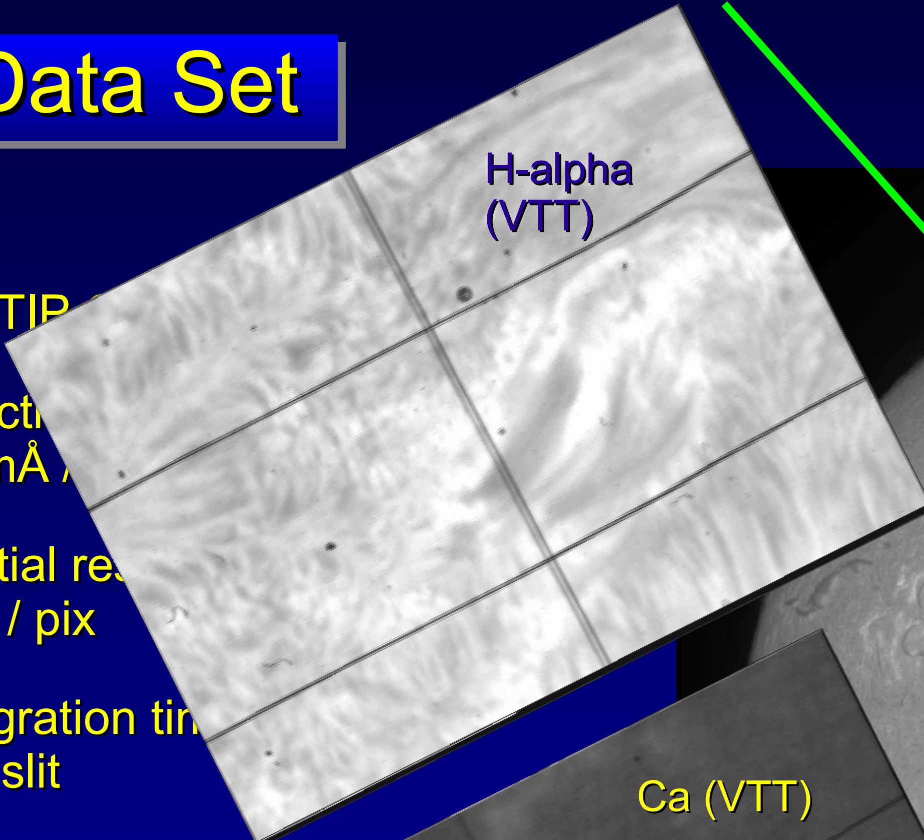

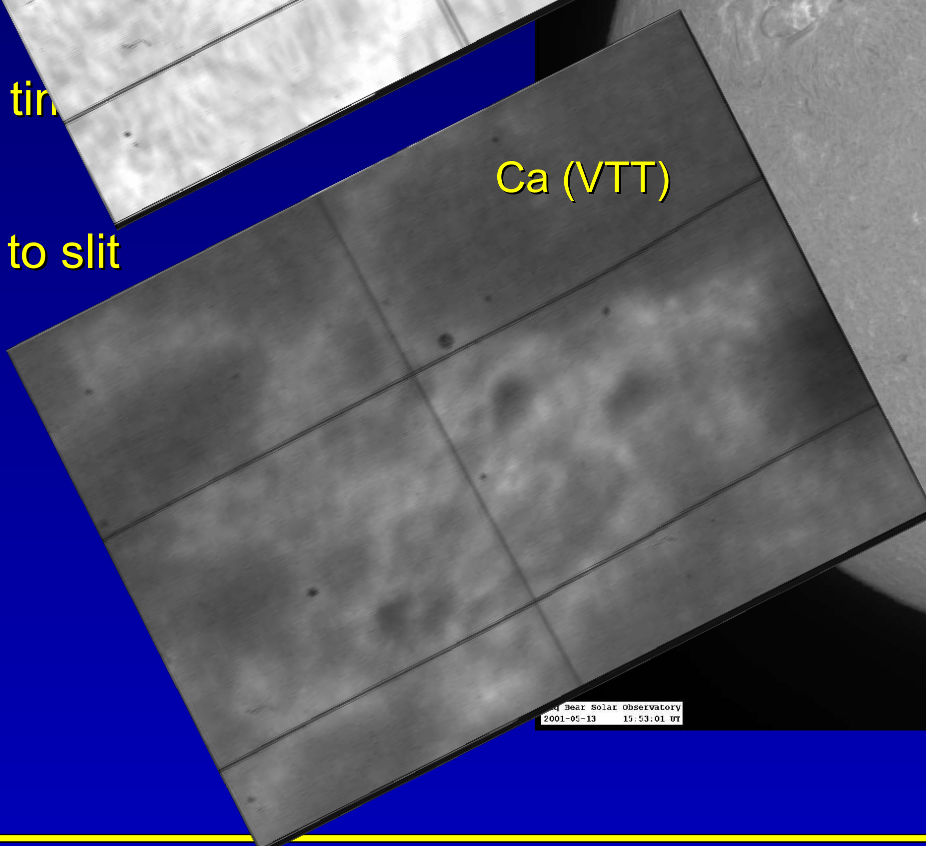

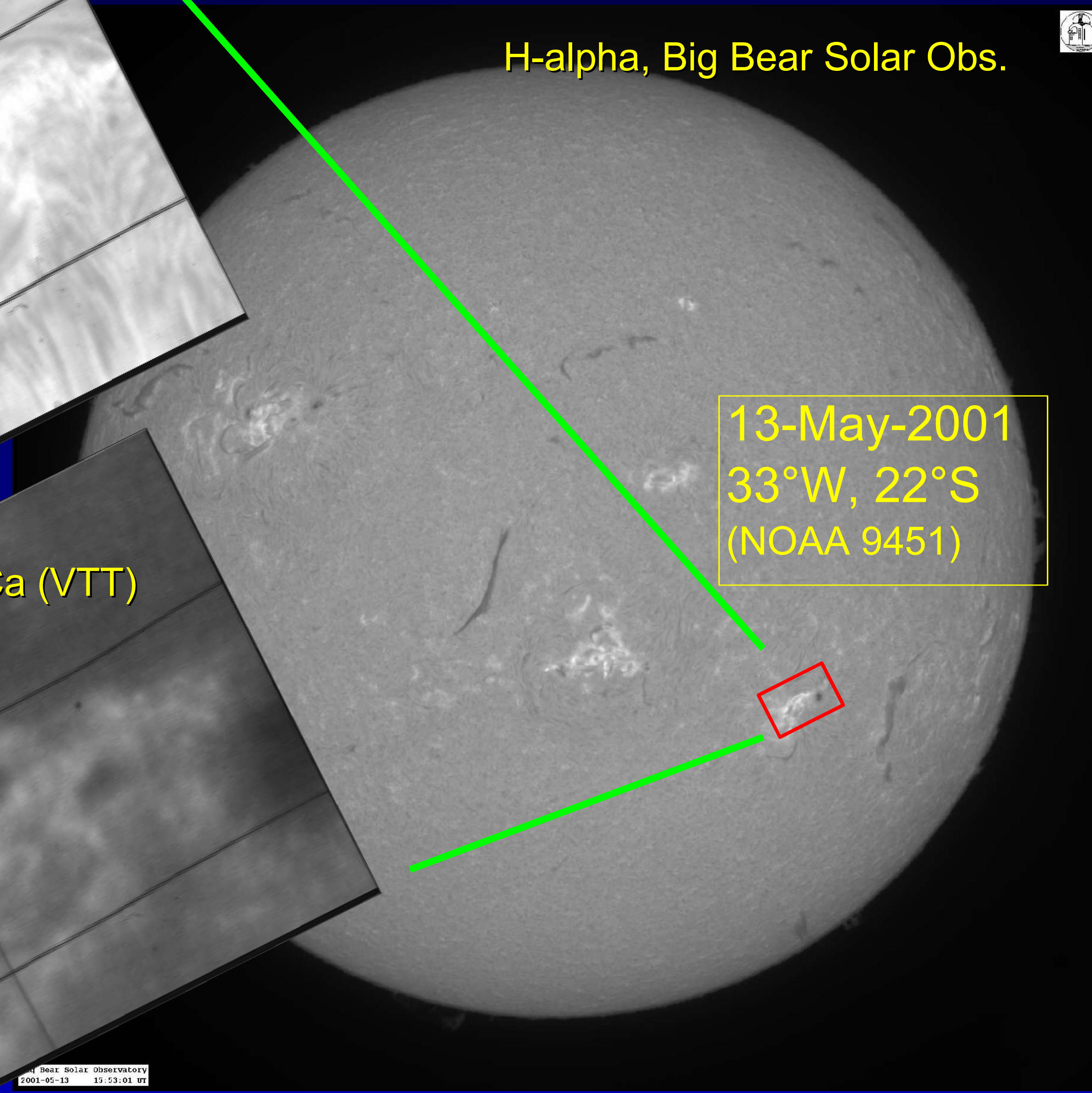

Observation

Photosphere, Si 10827

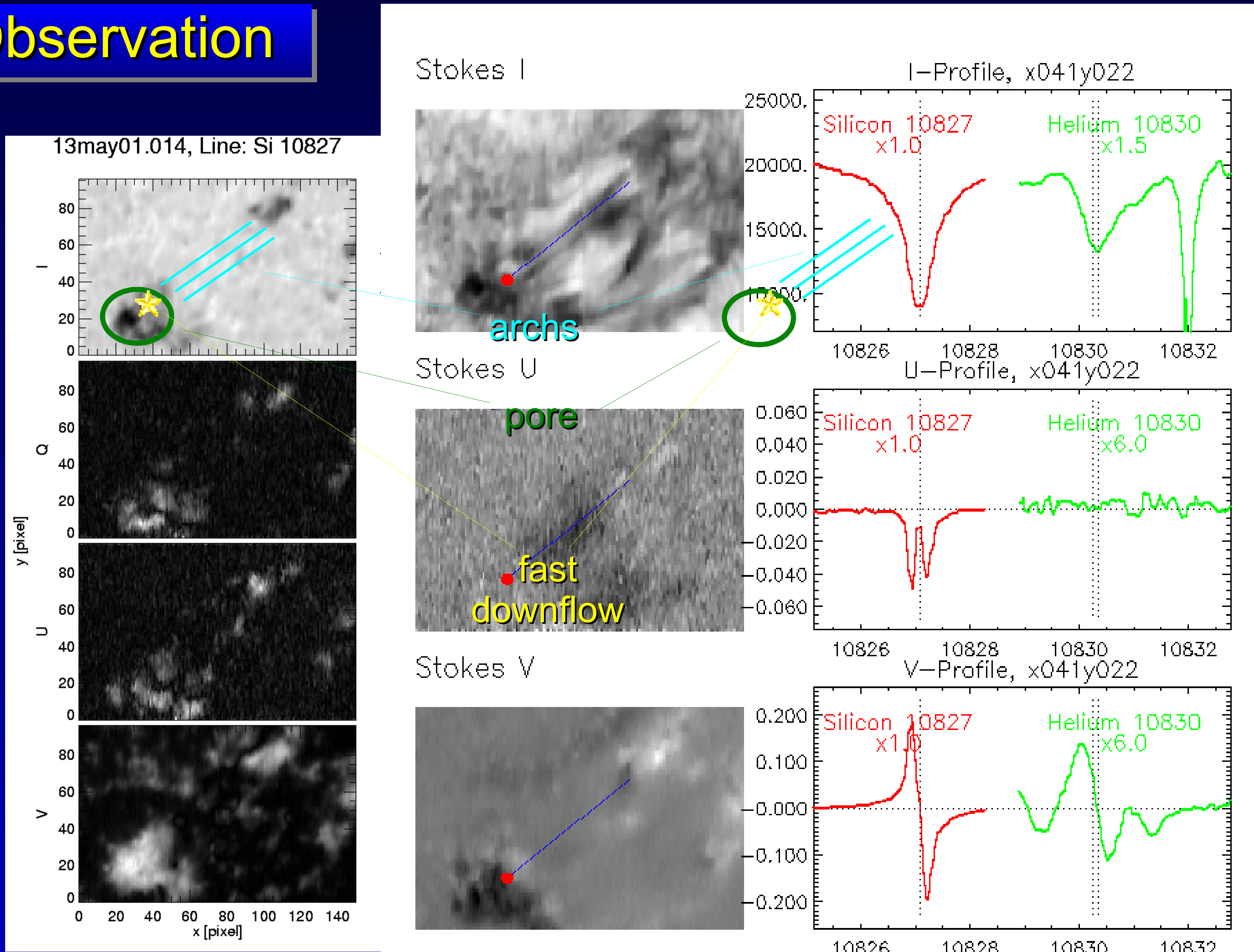

Magnetic Field Strength

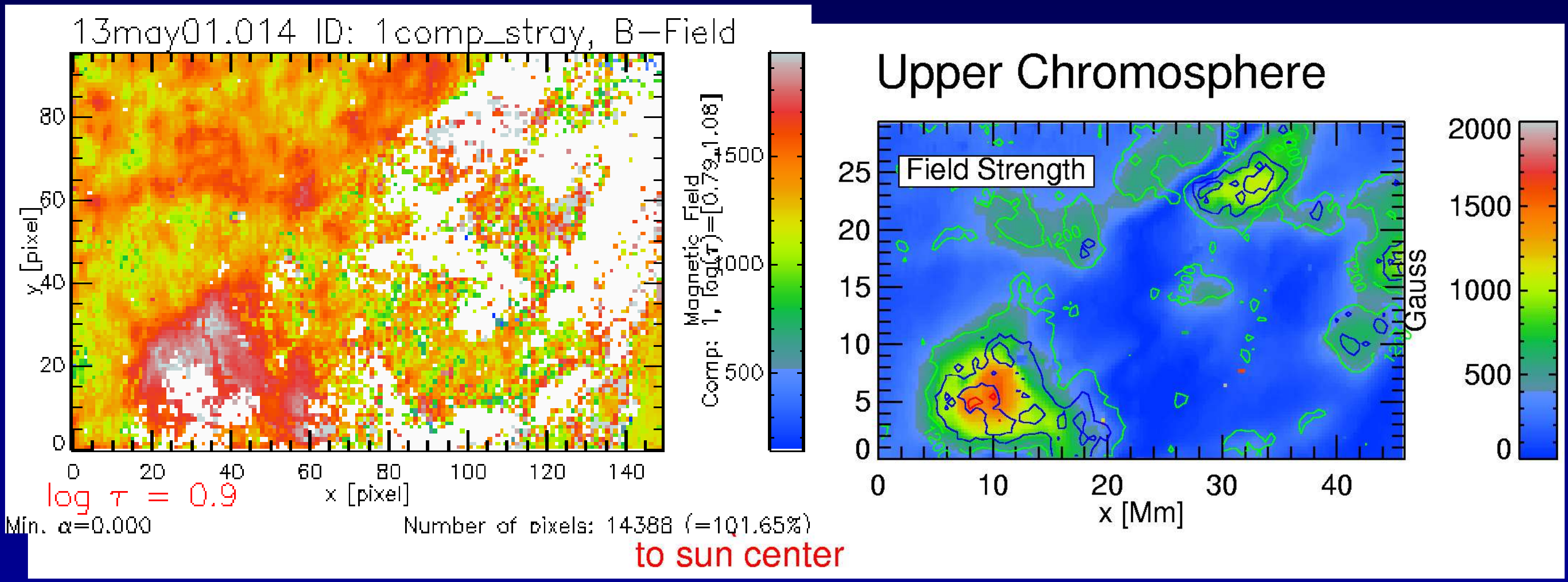

500-1000 G emerging flux region < 300 G

1000-2000 G surrounding 800-1500 G

Magnetic Field Direction

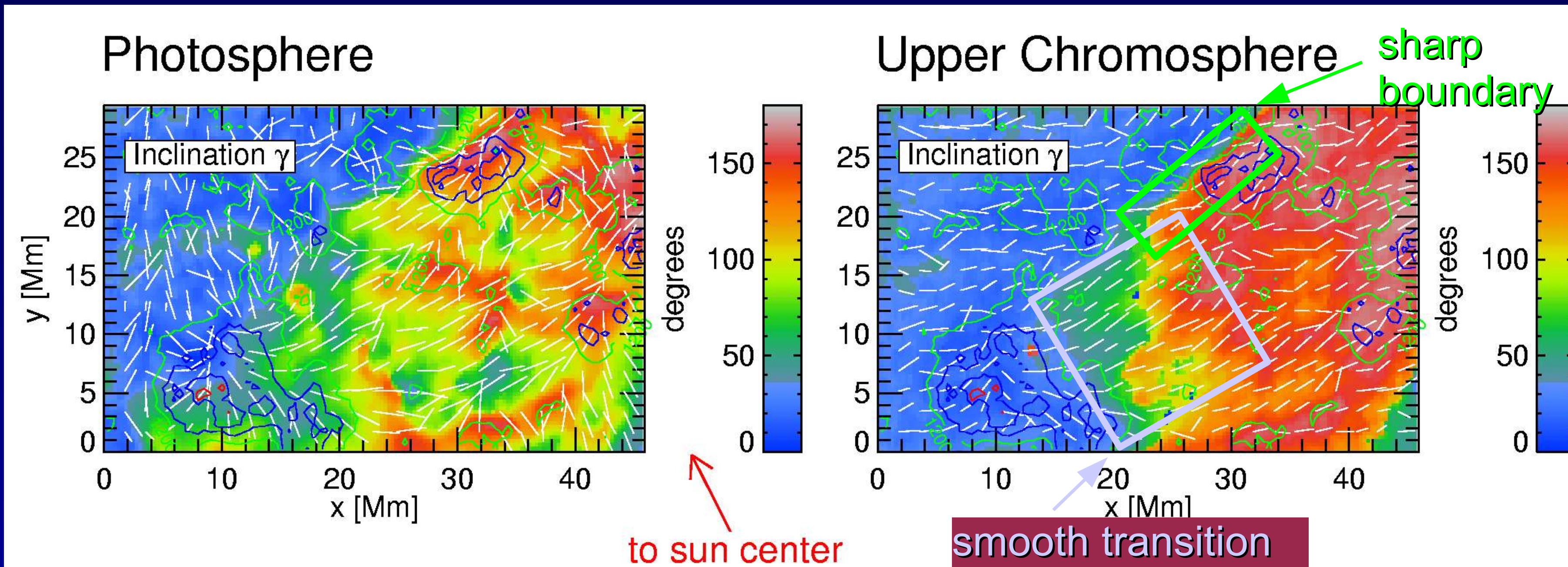

two polarities not connected in chromosphere
or
loops of extremely small horizontal extent

varying emerging flu

vertical surround

LOS Velocity

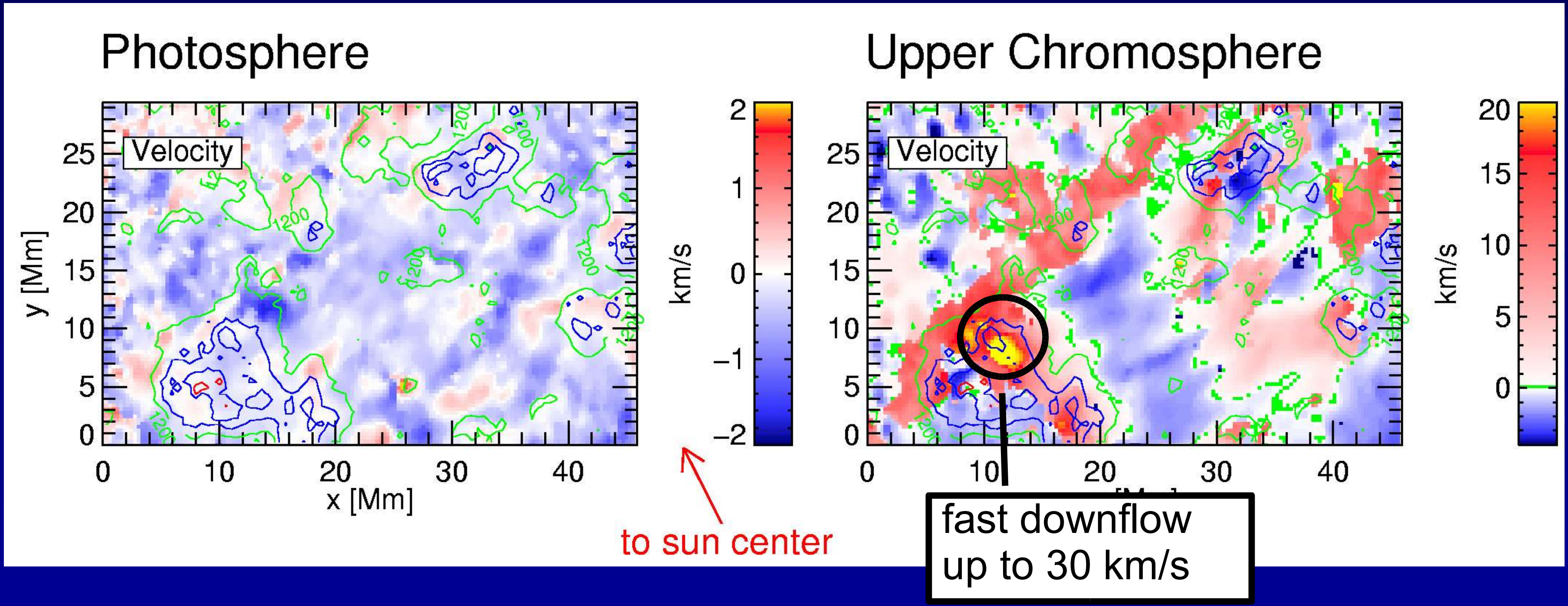

mainly upflow < 1 km/s	emerging flux region	upflow 0-4 km/s
up- and downflow < 2 km/s	surrounding	downflow 10-40 km/s

Loop Tracing

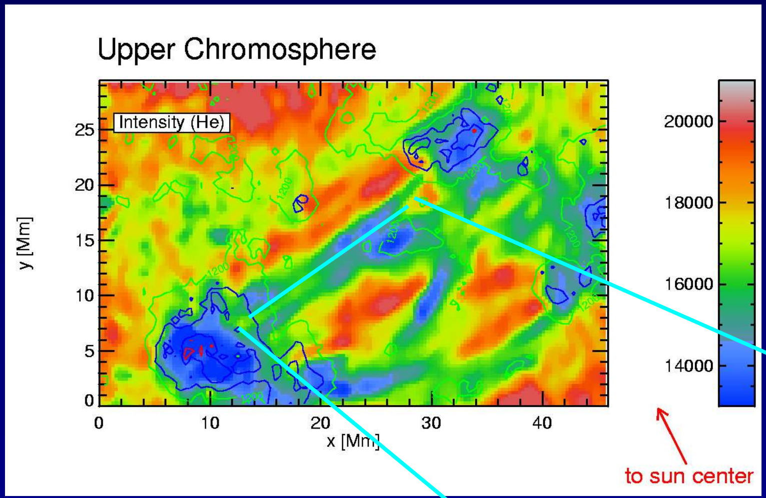

- start at random pixel
- connect to neighboring pixel using azimuth
- continue if pixel matches (direction, mag. field gradient)

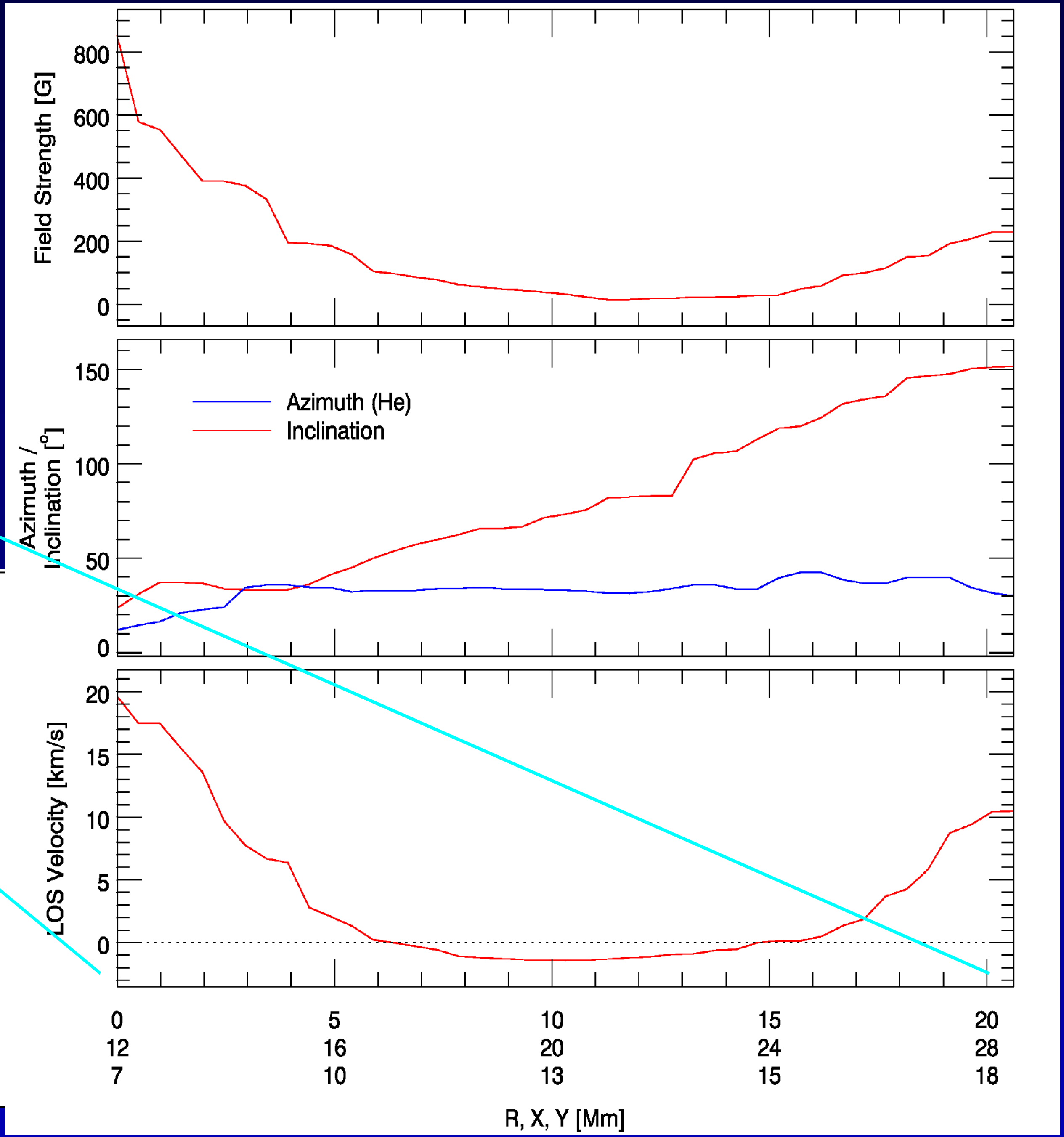

parameters of a "typical" loop

The 3-Dimensional Chromosphere

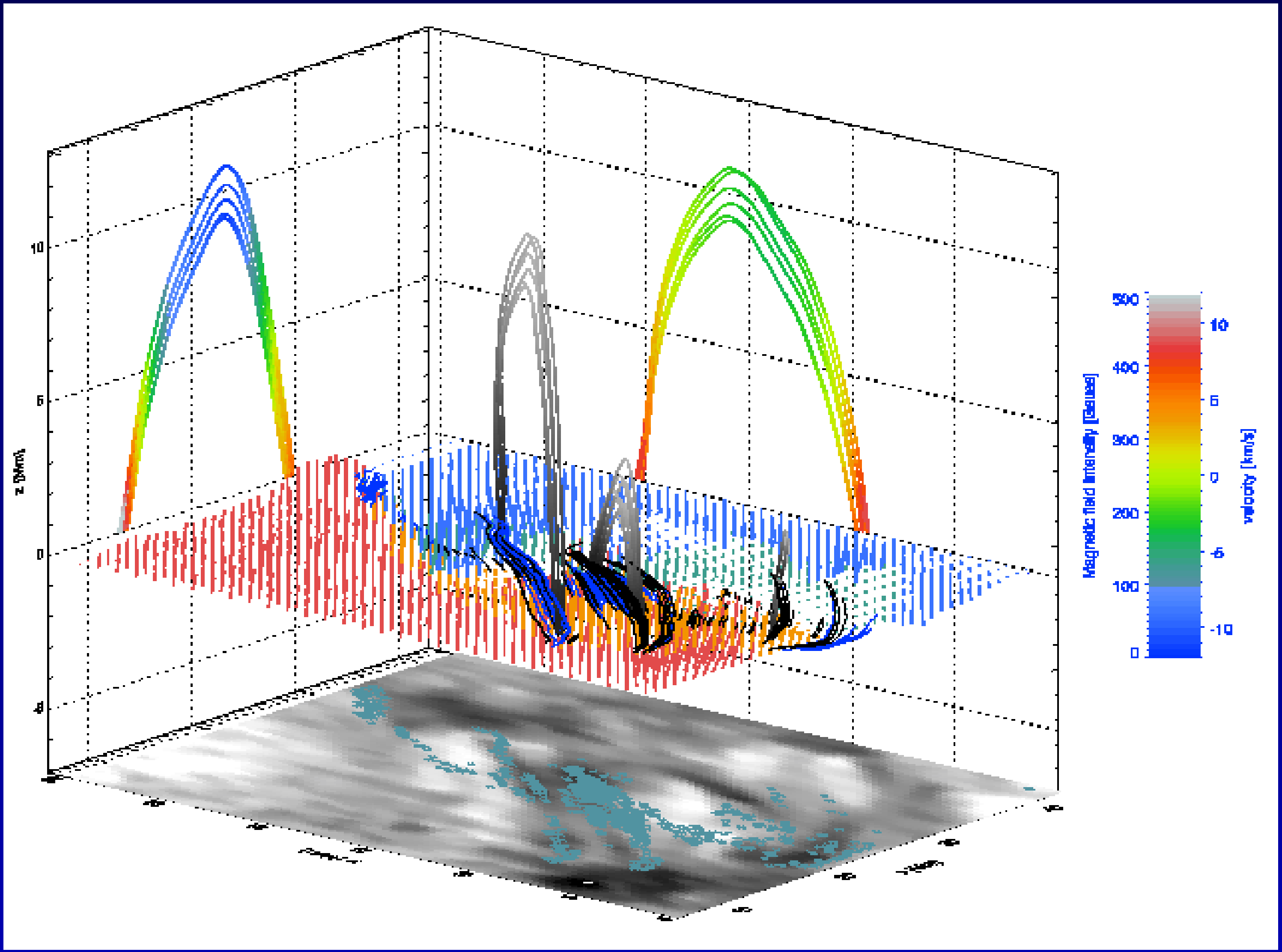

Comparison with Extrapolations

(T. Wiegelmann, 2003)

used map: photospheric field obtained from inversion of Si-line

force free field:

$$\nabla \times \vec{B} = \alpha B$$

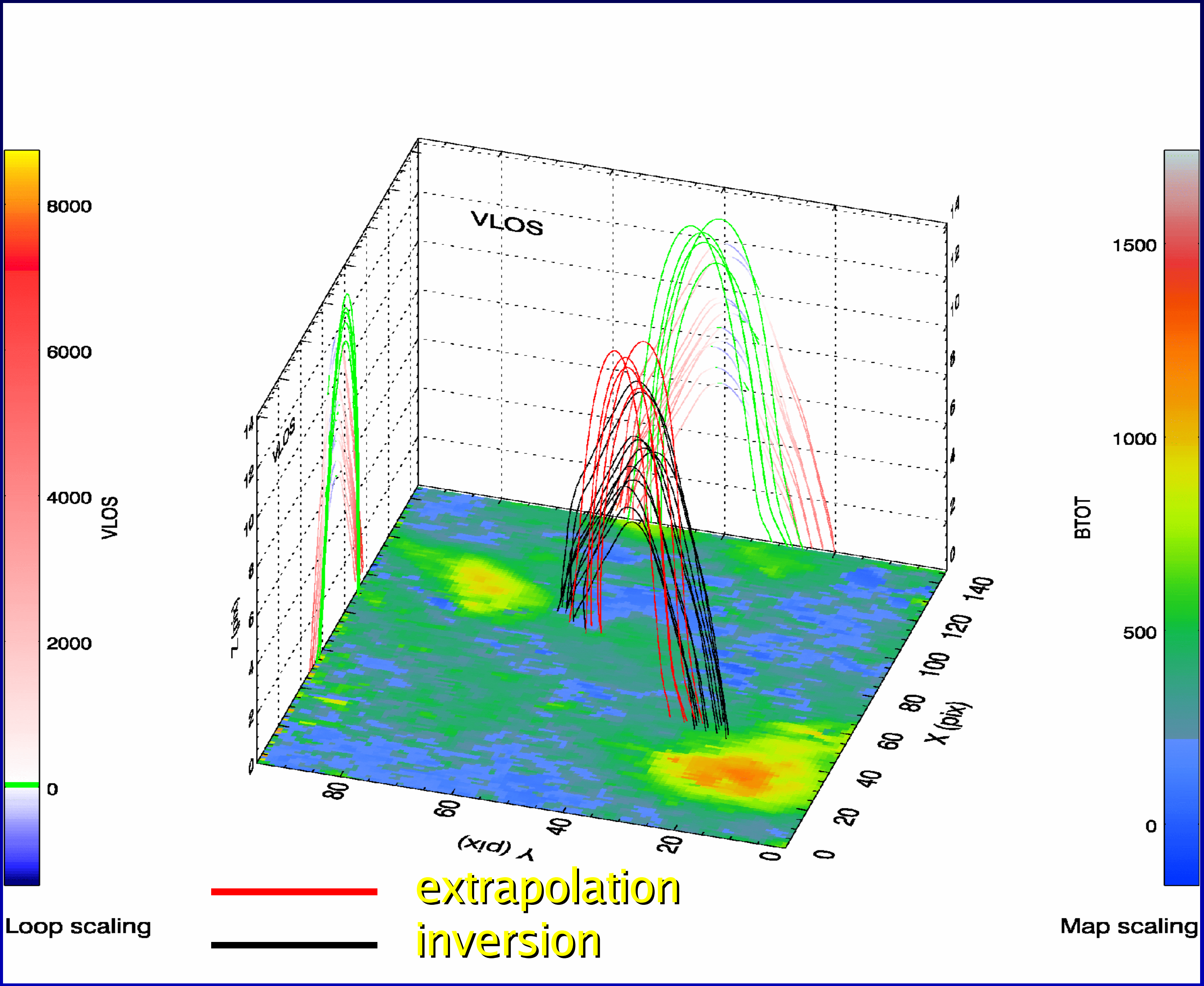

Current Sheet

- opposite polarity fields separated by < 4 pixels
- narrow valley (< 2Mm) where B < 50 G

→ electric current || surface

Ampère's Law:

$$j_{min} = 90 \text{ mA/m}^2$$

current sheet can continuously convert magnetic flux into heat and plasma kinetic energy

several C-Class events reported for NOAA 9451 on May 13 2001

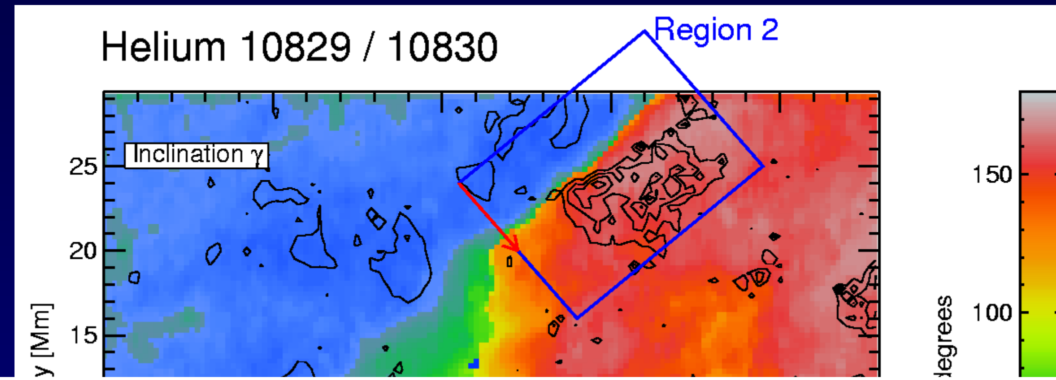

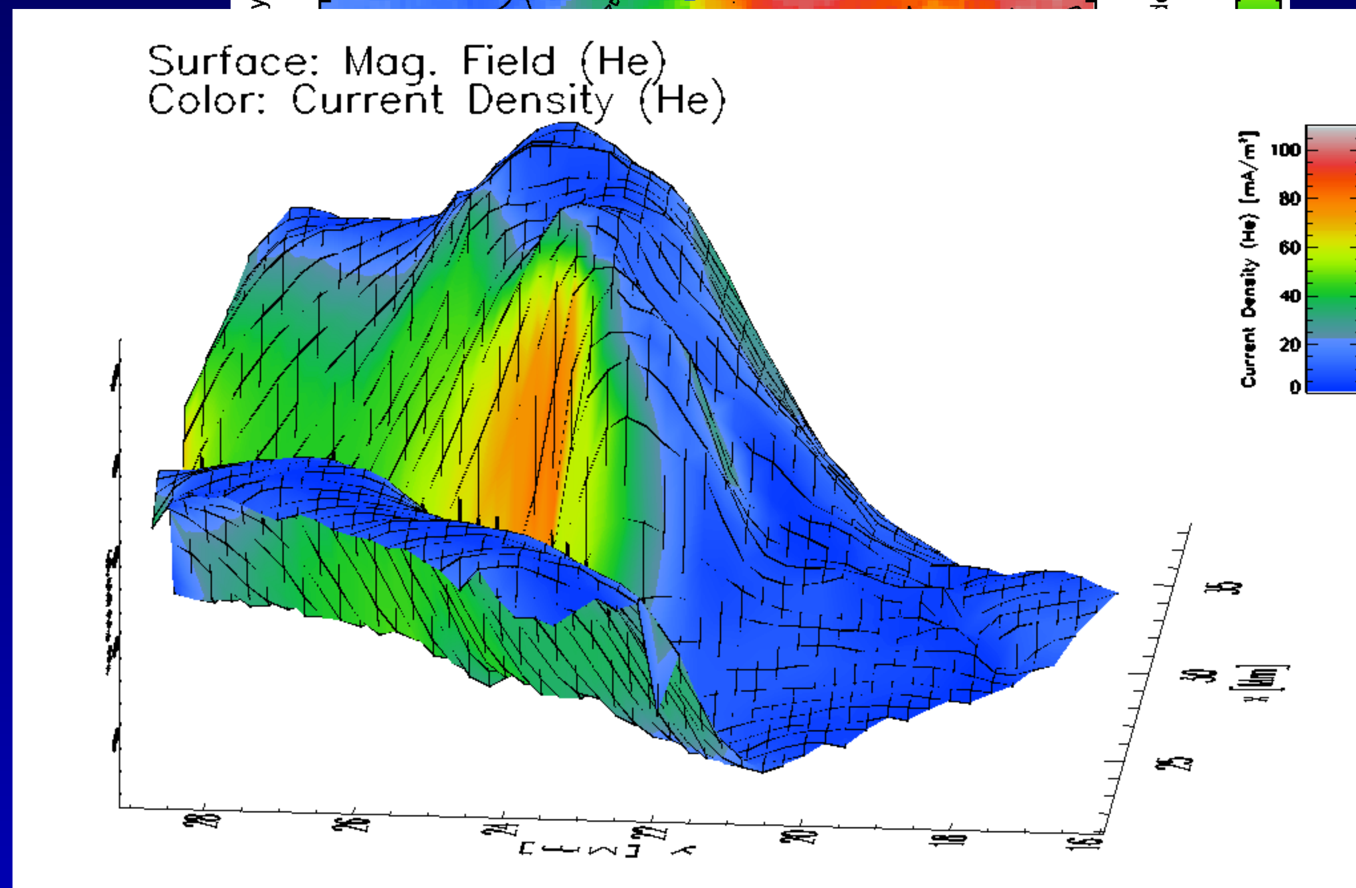

Solanki, Nature 2003

Downflows

very common feature: downflows of up to 60 km/s.

PIKAIA: allows the retrieval of magnetic field vector for slow and fast component

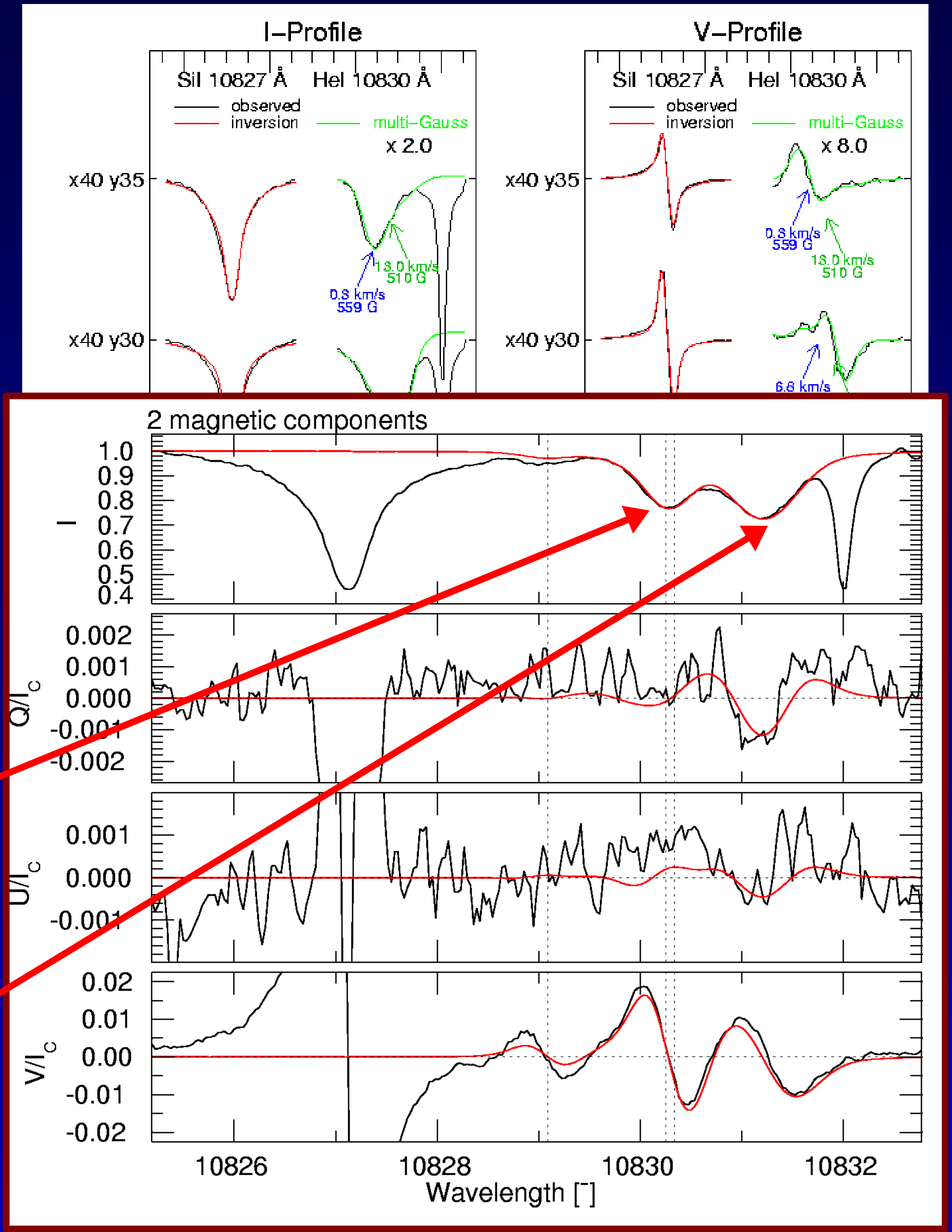

Slow Component:

VLOS	B	Incl.	Azim.
-620 m/s	520 G	33°	-14°

Fast Component:

VLOS	B	Incl.	Azim.
24900 m/s	730 G	67°	10°

Downflows – temporal evolution

~70 minutes

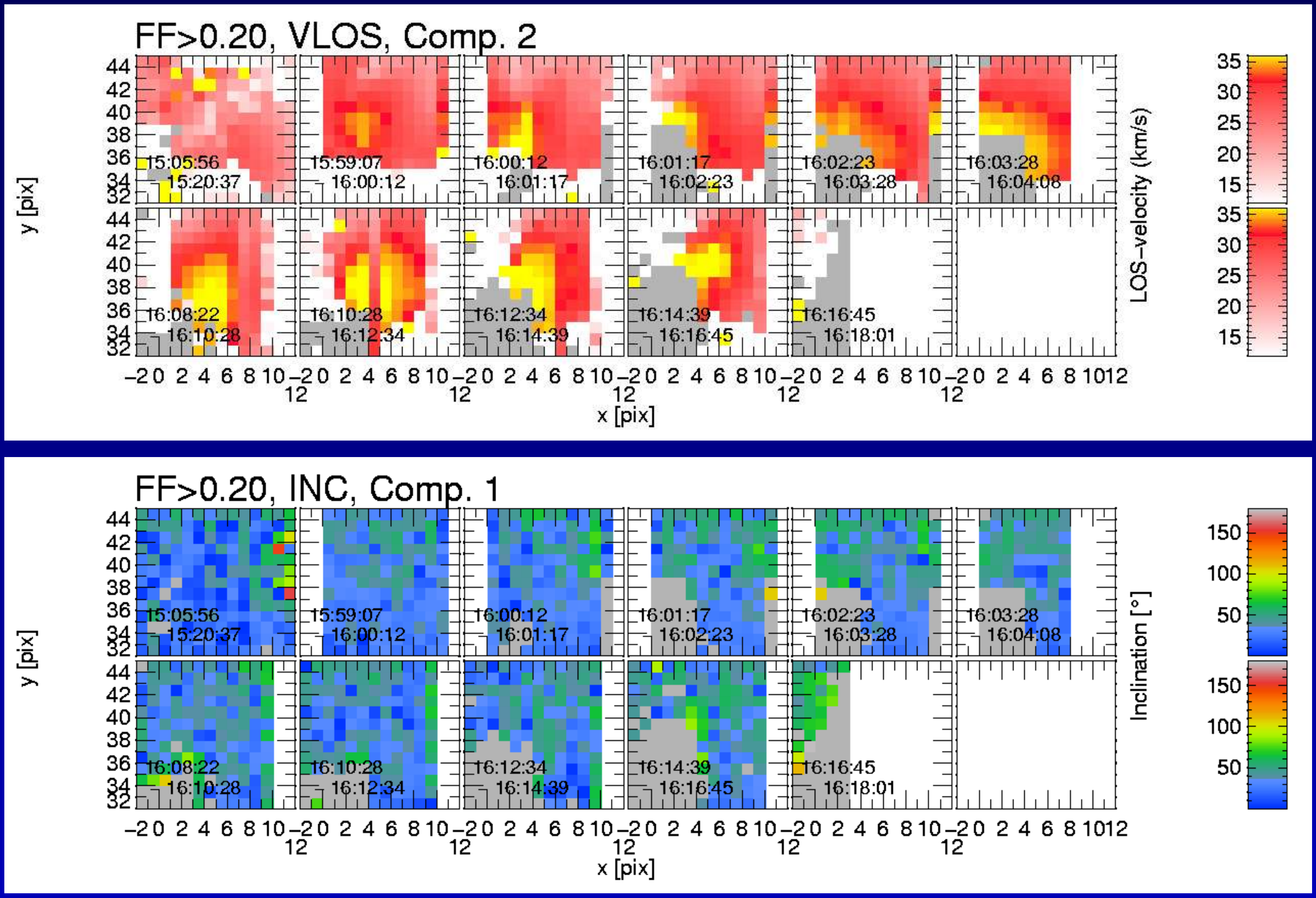

Uncombed chromosphere?

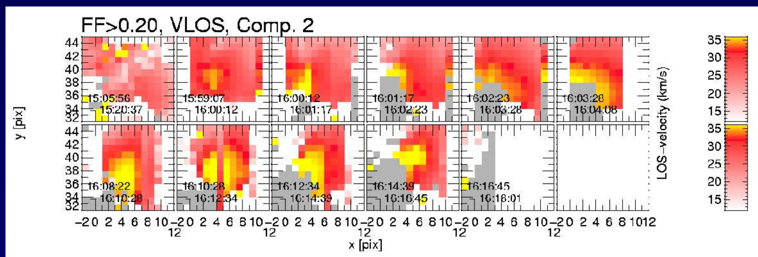

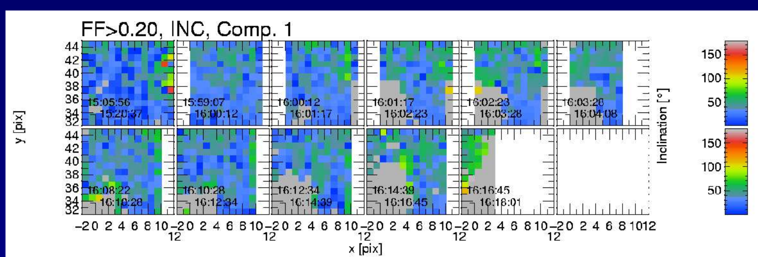

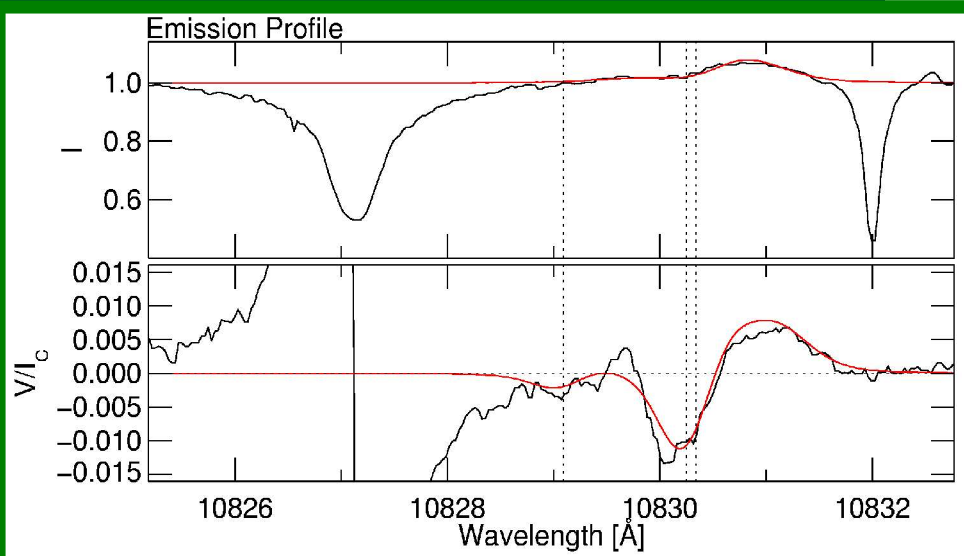

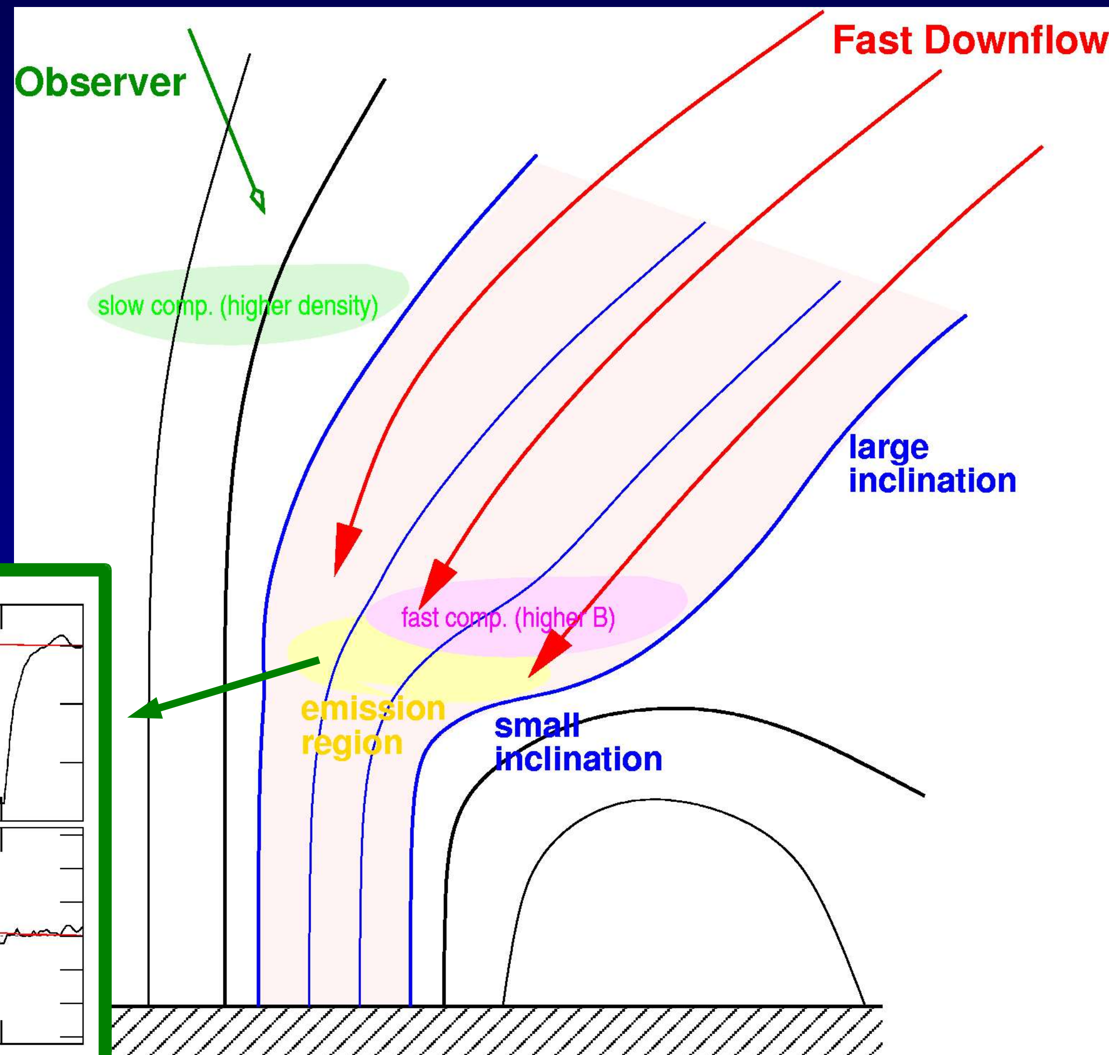

Properties of Emerging Flux Region

- magnetic field strength:
  - photosphere 500-1000 G
  - chromosphere <300 G
  - large magnetic field gradient (0.6 G/km)
- magnetic field orientation
  - large horizontal tubes in chromosphere
  - opposite polarity fields within pixel resolution (current sheet / tiny loops
  - horizontal / patchy in photosphere
- velocities:
  - slow upflow in photosphere and chromosphere
  - moderate / fast downflows at footpoints of arches in chromosphere
  - slow downflow at photospheric levels

→ Observations consistent with picture of emerging bipolar flux

Summary

- The near-infrared He I triplet is a unique diagnostic tool to investigate the upper chromosphere of the Sun - a region hardly accessible with other techniques. It allows the determination of the magnetic field vector and the line-of-sight velocity.
- In combination with the Si I line an emerging flux region could be observed at photospheric and chromospheric levels simultaneously.
- The height information resulting from the inversion smoothly connects the photospheric and the chromospheric level and is consistent with force-free field extrapolations
- The observations confirm the scenario of buoyantly rising flux transporting mass from the photosphere into the chromosphere and its drainage along arched magnetic loops.
- A tangential discontinuity in the magnetic field direction was interpreted as the signature of an electric current sheet. Such sheets can act as a source of coronal heating.

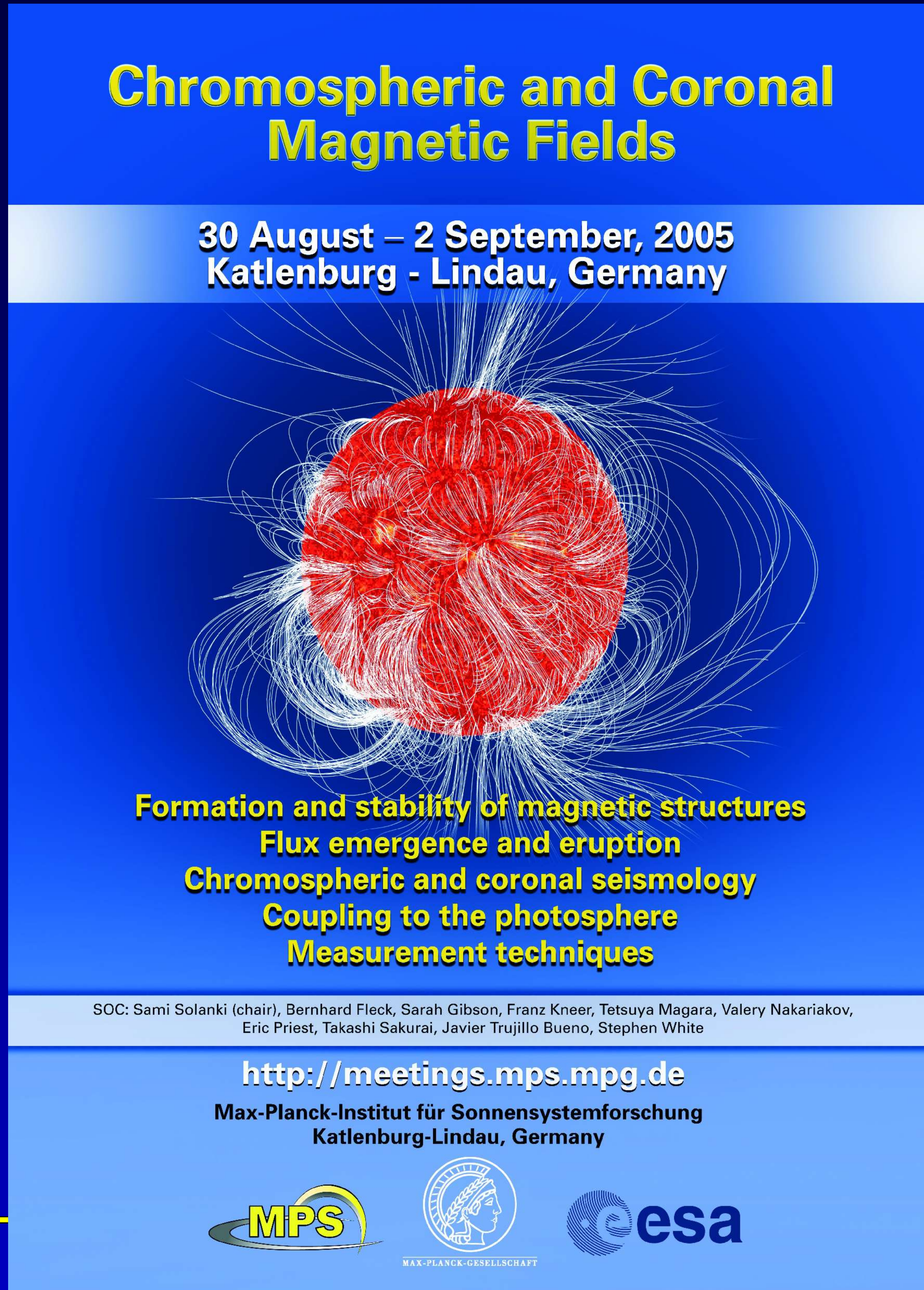
Chromospheric and Coronal Magnetic Fields
30 August – 2 September, 2005
Katlenburg - Lindau, Germany
Formation and stability of magnetic structures
Flux emergence and eruption
Chromospheric and coronal seismology
Coupling to the photosphere
Measurement techniques
SOC: Sami Solanki (chair), Bernhard Fleck, Sarah Gibson, Franz Kneer, Tetsuya Magara, Valery Nakariakov, Eric Priest, Takashi Sakurai, Javier Trujillo Bueno, Stephen White
http://meetings.mps.mpg.de
Max-Planck-Institut für Sonnensystemforschung
Katlenburg-Lindau, Germany
MPS
MAX-PLANCK-GESELLSCHAFT
esa